Förster energy transfer of dark excitons enhanced by a magnetic field in an ensemble of CdTe colloidal nanocrystals

Feng Liu,[1,2] A. V. Rodina,[3] D. R. Yakovlev,[1,3] A. A. Golovatenko,[3] A. Greilich,[1] E. D. Vakhtin,[4] A. Susha,[5] A. L. Rogach,[5] Yu. G. Kusrayev,[3] and M. Bayer[1,3]

[1]*Experimentelle Physik 2, Technische Universität Dortmund, 44221 Dortmund, Germany*
[2]*Department of Physics and Astronomy, University of Sheffield, Sheffield, S3 7RH, United Kingdom*
[3]*Ioffe Institute, Russian Academy of Sciences, 194021 St. Petersburg, Russia*
[4]*St. Petersburg State Polytechnical University, 195251 St. Petersburg, Russia*
[5]*City University of Hong Kong, Hong Kong*

(Received 9 July 2015; revised manuscript received 20 August 2015; published 4 September 2015)

We present a systematic experimental study along with theoretical modeling of the energy transfer in an ensemble of closely packed CdTe colloidal nanocrystals identified as the Förster resonant energy transfer (FRET). We prove that at low temperature of 4.2 K, mainly the ground dark exciton states in the initially excited small-size (donor) nanocrystals participate in the dipole-dipole FRET leading to additional excitation of the large-size (acceptor) nanocrystals. The FRET becomes possible due to the weak admixture of the bright exciton states to the dark states. The admixture takes place even in zero magnetic field and allows the radiative recombination of the dark excitons. An external magnetic field considerably enhances this admixture, thus increasing the energy transfer rate by a factor of 2–3 in a field of 15 T, as well as the radiative rates of the dark excitons in the donor and acceptor nanocrystals. The theoretical modeling allows us to determine the spectral dependence of the probability for the NC to serve as a donor for larger nanocrystals, to evaluate the energy transfer rates as well as to predict their dependencies on the magnetic field, to describe the spectral shift of the photoluminescence maximum due to the energy transfer, and to reproduce the experimentally observed spectral dependencies of the photoluminescence recombination dynamics in the magnetic field.

DOI: 10.1103/PhysRevB.92.125403 PACS number(s): 73.21.La, 78.47.jd, 78.55.Et, 78.67.Hc

I. INTRODUCTION

Colloidal semiconductor nanocrystals (NCs), and especially their optical properties, are attracting a lot of attention in very different fields [1–3]. A strong motivation here is related to promising applications ranging from light absorbers in photovoltaics and light emitters in optoelectronics to medicine and biology, where they can serve as efficient luminescent markers [4–7]. Due to the strong carrier confinement, NCs are appealing objects for basic research. They offer great variety of the structural parameters and engineering of the band gap profiles. It is possible to grow them as core-shell NCs of type-I or type-II band alignment, or synthesize NCs with different shapes, such as rods or platelets, which in turn can be combined in dot-in-rod or dot-in-plate structures [8]. Different potential applications of NCs are related to effects based on energy transfer in NC ensembles [9–11] and in their various hybrid structures [12–15]. At the same time, nonradiative energy transfer in an ensemble of closely spaced nanocrystals often leads to reduction of the photoluminescence (PL) quantum yield as compared to samples in solution [16].

Colloidal NCs are often based on II-VI semiconductors, e.g., CdSe, CdS, CdTe, ZnS, and their optical properties are dominated by the band edge excitons [17]. The exciton fine structure is controlled by the anisotropy of the crystal lattice and the nanocrystal shape as well as by the strong electron-hole exchange interaction that is enhanced due to the carrier confinement [17]. The lowest exciton state is optically forbidden in electric-dipole approximation for a one-photon process and is therefore referred to as a "dark exciton." The optically allowed "bright" exciton is shifted to higher energy by the exchange energy, which can be as large as a few meV. As a result, the recombination dynamics of NCs especially at low temperatures is nontrivial being dependent on the population of the dark and bright exciton states, the spin relaxation between them, and their mixing, e.g., in external magnetic fields.

In ensembles of closely packed NCs the phenomenology of recombination dynamics becomes even richer due to the energy transfer between the neighboring NCs. Due to the inhomogeneous broadening of the optical transitions caused by variations in NC size and shape, the NCs of smaller size emit in the high-energy flank of the spectrum and can serve as donor NCs as their energy can be transferred to the NCs of larger size (acceptor NCs), whose emission is shifted to the lower energy side of the spectrum. Experimentally the energy transfer is usually evidenced by the observation of spectral diffusion (i.e., a redshift of the PL spectrum with time) or by the observation of a spectral dependence of the photoluminescence dynamics, where the emission decay is shortened for the donor NCs. These findings have been reported for CdSe [18–26], CdS [27], CdTe [10,28–30], PbS [31], and Si [32] based nanostructures. It is well established and commonly accepted [12,33] that the most relevant mechanism of energy transfer (ET) in an ensemble of NCs with average diameter of 4–6 nm is the Förster resonant energy transfer (FRET) based on the nonradiative dipole-dipole coupling [34–37]. The Förster energy transfer rate Γ_{ET} can be described by the following equation [20,21]:

$$\Gamma_{\mathrm{ET}} = \frac{2\pi}{\hbar}\frac{(\mu_{\mathrm{d}}\mu_{\mathrm{a}}\kappa)^2}{R_{\mathrm{da}}^6 n^4}\Theta. \quad (1)$$

Here μ_{d} and μ_{a} are the transition dipole moments of excitons in the donor and acceptor NCs, respectively, κ is an orientational

factor (it accounts for the distribution of angles between the donor and the acceptor dipole moments; for random dipole orientation $\kappa^2 = 2/3$), R_{da} is the distance between donors and acceptors, n is the refractive index of the medium, and Θ is the overlap integral between the donor emission and the acceptor absorption spectra which are normalized to μ_d^2 and μ_a^2, respectively. It can be seen from Eq. (1) that $\Gamma_{ET} \propto 1/R_{da}^6$ is extremely sensitive to the distance between donor and acceptor NCs. The most efficient energy transfer corresponds to the situation for which two nanocrystals of different sizes are located in an immediate vicinity of each other and the ground state emitting level of the donor NC interacts resonantly with a higher lying absorbing level of the acceptor NC [21]. The nonradiative dipole-dipole energy transfer represents an additional effective channel for the decay and shortening of the PL lifetime in the donor NCs, which is caused by the interaction of the radiative dipoles in donor and acceptor NCs without emission and reabsorption of real photons. The radiative part of this interaction may also lead to energy transfer via emission and reabsorption of real photons as well as to a radiative correction to the donor radiative recombination rate. However, as it was shown recently [38], the radiative corrections to the radiative and energy transfer rates can be neglected for the typical spatial separation between the donor and acceptor dipoles at which the energy transfer is effective.

Thus, the important (dominating) role of the FRET for colloidal NCs is well documented and has been studied by continuous-wave and time-resolved photoluminescence. Most experiments have been performed at room temperature [20,21,32], with some low-temperature data being also available [24,39,40]. However, the details of the transfer mechanism at low temperatures, when the PL is governed by the emission from dark exciton state, as well as the possibilities to affect the efficiency of the energy transfer by external electric or magnetic fields, are not yet clarified and still open for detailed investigations.

So far, the FRET from semiconductor CdSe/CdS nanorods to dye molecules controlled by an electric field was demonstrated [41]. The responsible mechanism is based on the quantum confined Stark effect that enables a shift of the nanorod emission spectrum into resonance with the dye absorption band.

The effect of an external magnetic field on the FRET efficiency in colloidal NCs has not been studied systematically. There are two experimental papers related to this issue. Furis *et al.* [39] studied CdSe NCs in high magnetic fields up to 45 T. Pronounced exciton transfer via FRET was found in the spectrally resolved recombination dynamics. The magnetic-field-induced circular polarization degree of the PL was insensitive to the FRET process and the authors suggested that this may provide evidence for a spin-conserving FRET. The magnetic field effect on the FRET efficiency was not discussed, so no conclusion in this respect can be drawn from the presented experimental data. Blumling *et al.* [40] studied the effect of temperature and magnetic field on the energy transfer in CdSe NC aggregates by measuring the steady-state PL. The authors claimed that both temperature and magnetic field can enhance the energy transfer due to the population of the bright exciton state.

Theoretically, the dipole-dipole interaction mechanism for energy transfer and the influence of such factors as the donor-acceptor separation, the spectral overlap, and the effect of the surrounding [37,38,42] are well established. In contrast to multipole and exchange mechanisms [34,43], the direct dipole-dipole coupling conserves the spin of the participating charge carries. As the energy transfer rate depends on the dipole moments of the excitons in the donor and acceptor NCs, the dipole-dipole energy transfer has been considered to take place only between the bright exciton states. At the same time it is well established that the dark exciton states in colloidal nanocrystals are activated due to an admixture of bright exciton state wave functions [44]. This also means that the dark exciton states possess a nonzero dipole moment that is proportional to the admixed bright state dipole moment μ and the radiative lifetime of the dark exciton state is $\tau_F \propto 1/\mu^2$. Up to now, the possibility of FRET between dark excitons has been analyzed neither theoretically nor experimentally.

A quantitative analysis of the energy transfer rates from experimental data is complicated by several factors. Usually the rates are extracted from the comparison of luminescence decay curves for small NCs (donors) that participate and do not participate in the transfer process [20,21,32]. However, the donor decay curves are usually strongly nonexponential due to the inhomogeneous spatial distribution of acceptors around the donors. Theoretical modeling of the time evolution of donor and acceptor populations in a mixed ensemble of CdSe NCs has been done in Refs. [18,19] and reproduced the observed spectra well. However, this analysis has not taken into account the exciton fine structure and the possibility of the dark exciton states to contribute to the energy transfer process.

In this paper we report an experimental and theoretical study of the energy transfer in an ensemble of closely packed CdTe NCs. The energy transfer is evidenced experimentally by the time-dependent shift of the PL maximum after pulsed excitation. The observed shift is well described theoretically by the energy transfer between small and large NCs. An important observation concerns the time scale of the process—at low temperatures the energy shift is observed during times much longer than the lifetime of the bright exciton that is shortened by the fast thermalization due to the relaxation to the dark exciton state. Spectrally and temporally resolved photoluminescence measurements reveal a strong spectral dispersion of the exciton lifetime and give clear evidence of a second rise of the PL intensity (after the initial decay) at the low energy side of the spectrum that becomes enhanced in an applied magnetic field. Our theoretical modeling of the donor and acceptor population takes into account the exciton fine structure and the possibility of dipole-dipole energy transfer from the dark exciton state. The results of the simulations reproduce the observed emission decays of the acceptor NCs and allow us to determine all parameters of the energy transfer process and their dependence on the magnetic field. The energy transfer rate from the dark exciton increases in the external magnetic field due to the increase of the dipole moments in both the donor and acceptor NCs.

The paper is organized as follows: Sec. II gives a description of the samples and experimental conditions. The experimental data with an emphasis on evidencing the energy transfer process are presented in Sec. III. The theoretical considerations

and the resulting modeling of the experimental data are presented in Secs. IV and V, respectively. The main conclusions are summarized in Sec. VI.

II. EXPERIMENT

Thiol-capped CdTe colloidal NCs were synthesized in water as described in Ref. [45]. The exciton recombination and spin relaxation dynamics in such NCs were reported in Ref. [46]. In this work, two samples with average core diameters of 3.4 and 3.7 nm were studied. For the optical experiments at cryogenic temperatures aqueous solutions of CdTe NCs were drop-casted on a glass slice and dried. The resulting films consist of areas of NCs with varying (high and low) in-plane densities of NCs, which are characterized by high and low total PL intensities, respectively. These inhomogeneous films allow us to study and compare the effect of the energy transfer on the ensemble PL spectrum and PL dynamics for areas with different average spatial separation between NCs and thus different values of R_{da} determining the transfer rate.

The samples were inserted into a cryostat equipped with a 15 T superconducting magnet. The magnetic field **B** was applied in the Faraday geometry, it was oriented perpendicular to the glass slice and parallel to the light wave vector. The sample was in contact with helium gas and the bath temperature was varied from $T = 4.2$ up to 300 K.

Photoluminescence was excited and collected through multimode optical fibers. The collected emission was dispersed with a 0.55-m spectrometer. Time-integrated PL spectra were measured for continuous-wave (cw) laser excitation with a photon energy of 3.33 eV (wavelength 372 nm) and detected with a liquid-nitrogen-cooled charge-coupled-device camera. We denote them as steady-state PL spectra.

For time-resolved measurements the samples were excited with picosecond laser pulses (photon energy 3.06 eV, wavelength 405 nm, pulse duration 50 ps, repetition frequency 150 to 500 kHz). The PL signal was sent through the spectrometer and detected by an avalanche photodiode (time response 50 ps) connected to a standard time-correlated single-photon counting module. The instrument response function of the setup was better than 800 ps. All measurements were performed at low excitation densities of 0.1 mW/cm^2 to avoid any multiexcitonic contribution to the emission spectra.

III. EXPERIMENTAL RESULTS

A. Steady-state PL spectra and spectrally integrated recombination dynamics

Steady-state PL spectra of the 3.4 and 3.7 nm CdTe NCs measured under cw excitation at $T = 4.2$ K are shown in Fig. 1(a). Their peak positions are at 1.99 eV for the 3.4 nm NCs and 1.83 eV for the 3.7 nm NCs. The spectra of both samples are rather broad with a full width at half-maximum (FWHM) of ~120 meV, which evidences the considerable NC size dispersion of about 7%.

The exciton recombination dynamics in the NCs can be characterized by the spectrally integrated time-resolved PL. Figure 1(b) shows the integral PL decay obtained by summing up the PL decays measured at 20 energies distributed across

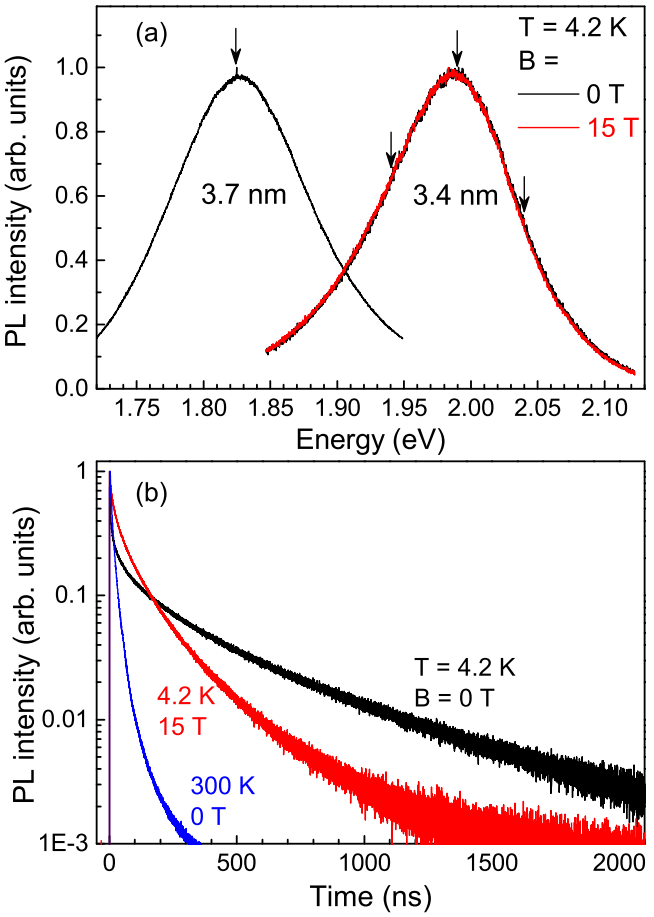

FIG. 1. (Color online) (a) Normalized steady-state PL spectra of the 3.4 and 3.7 nm CdTe NCs measured at $T = 4.2$ K in zero magnetic field $B = 0$ T (black lines) and at $B = 15$ T (red line). The arrows indicate the energies at which the PL dynamics shown in Figs. 7 and 8 are measured. (b) Recombination dynamics of the spectrally integrated PL intensity in the 3.4 nm CdTe NCs measured at $T = 4.2$ K in magnetic fields of $B = 0$ T (black line) and $B = 15$ T (red line), and at $T = 300$ K (blue line).

the whole PL band of the 3.4 nm NCs. At room temperature the PL decay can be described by a biexponential function with decay times of 6 and 22 ns. The longer component originates from the thermally mixed bright and dark exciton states. With decreasing temperature down to 4.2 K the decay shows a multiexponential behavior due to the exciton thermalization into the optically forbidden (dark) state, which is the lowest exciton state in NCs. It is well established that the very fast initial decay with a time of approximately 2 ns is related to the optically allowed (bright) exciton. Its decay is dominated by the fast scattering from the bright to the dark state and has some contribution from the radiative recombination of bright excitons [47–49]. The slow component with a decay time of about 260 ns corresponds to the lifetime of the dark (optically forbidden) exciton τ_F, whose recombination becomes partially allowed due to a weak mixing of the dark and the bright exciton states caused, e.g., by the magnetic moments of dangling bonds at NC imperfections and surface states.

An external magnetic field induces a mixing of the bright and the dark exciton states, which results in the vanishing

of the fast decay component and the shortening of the slow component. Such a behavior, well established for CdSe and CdTe NCs [47,50], is observed also for the studied sample. In a magnetic field of 15 T the amplitude of the fast component ultimately vanishes and the slow component is shortened down to about 100 ns, compare the red and black curves in Fig. 1(b).

B. Evidence for the energy transfer process: Spectral diffusion

We now turn to the experimental results that evidence on the energy transfer in the studied CdTe NC solids. Figure 2(a) compares the steady-state (solid lines) and the time-resolved (lines with dots) PL spectra of the 3.4 nm NCs measured at zero time delay just after the excitation pulse. The red and black lines show the results measured at two different sample areas with different NC densities, high and low, respectively.

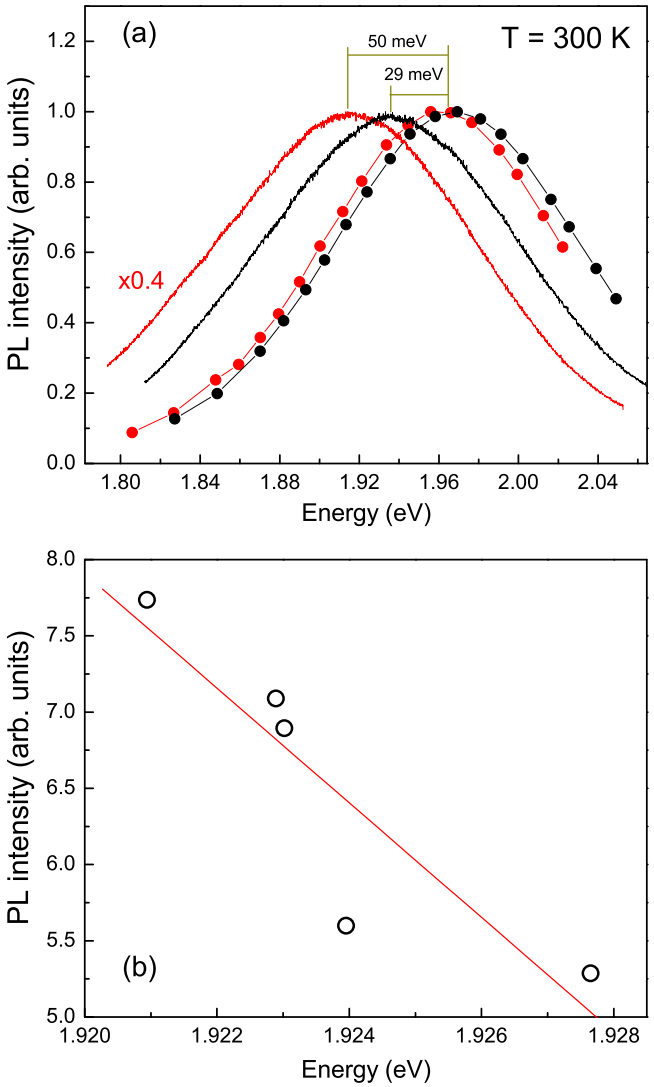

FIG. 2. (Color online) (a) Normalized time-resolved (lines with dots) and steady-state (solid lines) PL spectra measured at high-density (red) and low-density (black) areas of the sample with 3.4 nm CdTe NCs. (b) PL intensity versus peak position of the steady-state PL spectra measured at areas with different densities of CdTe NCs. The line is a linear interpolation.

The PL intensities at these points differ by a factor of 2.5. The time-resolved spectra from these high- and low-density areas are similar to each other, indicating the same NC size dispersion in these areas. Note that these spectra, measured right after the pulse, are not contributed by the energy transfer and, therefore, give us information on the density of states in the NC ensemble.

The steady-state PL spectra in Fig. 2(a) are shifted to lower energies compared to the time-resolved spectra. This shift is larger in the area with higher NC densities reaching 50 meV compared to 29 meV in the high- and low-density areas, respectively. In general, such shifts may be induced by the energy transfer, but also the spectral dependence of the PL dynamics across the emission band may be a possible origin. As the second reason is not relevant for CdTe NCs [28], we attribute the shift solely to the energy transfer. The higher density of NCs corresponds to a smaller separation between them. Therefore, for the higher NC density the FRET is more efficient and, consequently, a lager shift between time-resolved and steady-state PL spectra is expected.

A systematic correlation between the NC density and the energy shift of the steady-state PL spectra measured at different sample areas is shown in Fig. 2(b). Here the PL intensity from the sample areas with different NC densities is plotted against the peak energy. One can see that stronger PL intensities correspond to the areas with lower peak energy, i.e., larger shift. This correlation agrees with the expectations from the Förster mechanism for the energy transfer and is in line with the experimental data reported in Ref. [30].

The time evolution of the PL spectra measured in high density areas at different time delays is presented in Fig. 3 for temperatures of 4.2 and 300 K. The strong spectral shift with increasing delay is prominent at both temperatures. For comparison, the steady-state PL spectra are also shown by the solid red lines. At $T = 4.2$ K the emission intensity decreases with time monotonically and the maximum of the spectrally resolved PL spectra shifts from 2.05 eV at $t = 0$ ns down to 2.01 eV at 70 ns, see Fig. 3(a). A similar behavior is observed at room temperature, where the time-resolved spectra shift from 1.96 eV at 0 ns down to 1.92 eV at 70 ns. An important feature related to the energy transfer is seen at room temperature in Fig. 3(b). Namely, the PL intensity varies nonmonotonically at the low energy tail of the emission band. It increases during several nanoseconds after the excitation pulse and only then starts to decay. This behavior will be shown in more detail below where the PL dynamics measured at different spectral energies are presented.

Figure 4 shows shifts of the PL maxima with time, measured at two sample areas having similar PL intensities. Due to the sample inhomogeneity several experimental data sets were measured at different sample areas. The characteristic behavior is, however, well reproducible for all these areas. For area 1 the PL spectrum shifts by 47 meV during the first 70 ns at $T = 4.2$ K, see Fig. 4(a). The shift becomes larger with increasing temperature and reaches 75 meV at 300 K, indicating a more efficient energy transfer. In both cases the fast initial energy shift during the first 10 ns is then gradually slowed down with a tendency to saturated. A similar shift of the PL maximum was presented in Refs. [20,21,25] and attributed to the energy transfer process at room temperature.

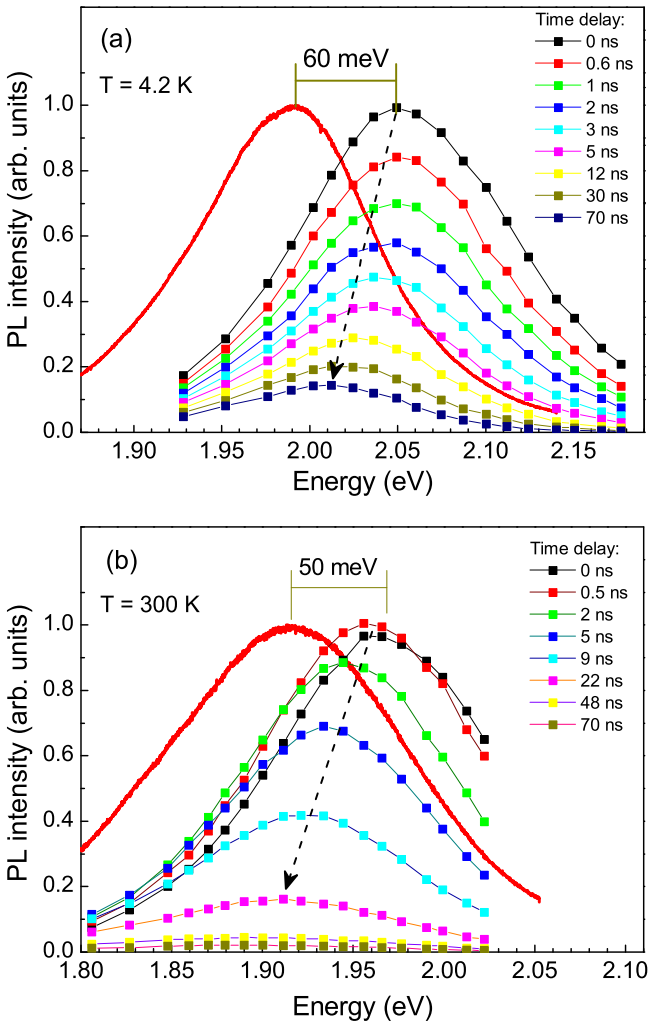

FIG. 3. (Color online) Steady-state PL spectra (solid red lines) and time-resolved PL spectra (lines with dots) of the 3.4 nm CdTe NCs measured at (a) $T = 4.2$ K and (b) 300 K.

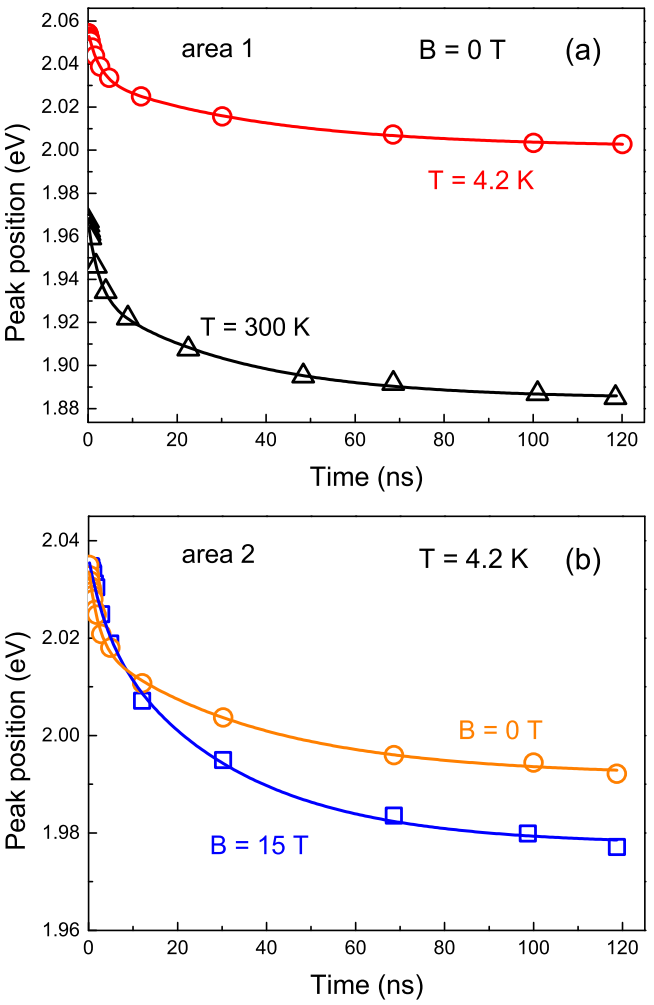

FIG. 4. (Color online) Temporal shift of the PL maximum in 3.4 nm CdTe NCs measured for two sample areas at different temperatures and magnetic fields. The experimental data are shown by symbols. Lines are fits according to Eq. (2).

It should be noted that the spectral shift (the spectral diffusion) can be also observed in systems without any energy transfer, for example in the donor-acceptor pair recombination in bulk semiconductors [51]. In this case the spectral diffusion is caused by the spectral dependence (dispersion) of the recombination rates. However, for CdTe NCs no dispersion of the recombination dynamics was found in an ensemble of noninteracting NCs, i.e., in the absence of energy transfer [28]. In addition, we observed the same correlation between the temporal shift of the PL maxima and the PL intensity as for the shift of the cw spectral maxima: the areas with larger PL intensity and thus higher NC density demonstrate a larger temporal shift of the PL maximum. Therefore, we attribute the observed spectral shift solely to the effect of the energy transfer.

It is important to note that at $T = 4.2$ K the bright excitons in our NCs scatter to the dark states during 2 ns, see Fig. 1(b). But the energy transfer occurs at much longer times. Therefore, it cannot be provided by the FRET involving the bright excitons. This evidences that the dark excitons can play an important role in the energy transfer. We will discuss this below in more detail.

From Fig. 4(b) is can be seen that application of an external magnetic field enhances the energy transfer. The PL spectrum shift during the first 70 ns measured at $B = 15$ T (51 meV) is larger than that measured at 0 T (40 meV). This is in contrast to the shift of the cw spectra which is independent of the magnetic field, as can be seen from comparison of the cw spectra at $B = 0$ and 15 T in Fig. 2(a). Commonly, the magnetic field enhances the carrier localization and shrinks the exciton wave function. Therefore, the energy transfer mechanisms involving tunneling of excitons or carriers between NCs are expected to be slowed down in a magnetic field. But not the FRET, which can be enhanced by, e.g., the magnetic field induced increase of the exciton oscillator strength.

The solid lines in Fig. 4 are fits using a form similar to that in Refs. [24,25]:

$$E(t) = E_0 + \Delta E_1(e^{-t\Gamma_{\Delta E_1}} - 1) + \Delta E_2(e^{-t\Gamma_{\Delta E_2}} - 1). \quad (2)$$

TABLE I. Fit parameters for modeling the time evolution of the PL peak maximum according to Eq. (2).

Area condition	E_0 (eV)	ΔE_1 (meV)	$\Gamma_{\Delta E_1}$ (ns^{-1})	ΔE_2 (meV)	$\Gamma_{\Delta E_2}$ (ns^{-1})
Area 1 4.2 K, 0 T	2.055	22	0.38	32	0.025
Area 1 300 K, 0 T	1.967	34	0.41	48	0.031
Area 2 4.2 K, 0 T	2.035	16	0.45	27	0.027
Area 2 4.2 K, 15 T	2.036	14	0.23	45	0.033

The parameters of the fits, the shift energies $\Delta E_{1,2}$, and the shift rates $\Gamma_{\Delta E_{1,2}}$ are given in Table I. We note that the fitting with only one characteristic shift rate does not work well: in all cases the first initial fast energy shift is followed by a slow shift. We comment on the physical meaning of the different shift rates in the theory Sec. V C.

C. Evidence for the energy transfer process: Spectrally resolved PL dynamics influenced by an external magnetic field

Figure 5 shows the spectrally resolved PL dynamics of the 3.4 nm CdTe NCs measured at $T = 4.2$ K. At zero magnetic field, the PL decay shows a multiexponential behavior. At the high energy side of the emission band, e.g., at 2.08 eV (black line), the decay starts with fast components of 1 and 4 ns that are followed by an intermediate component of 30 ns finally turning to a very slow component with 320 ns decay time. The relative contribution of the intermediate component decreases for lower spectral energies, whereas the slow component is spectrally independent. The fast component can be attributed to bright excitons, namely to their radiative recombination and scattering to the dark states. The intermediate component is most likely related to the FRET from smaller to larger NCs. The slow component is due to the recombination of dark excitons.

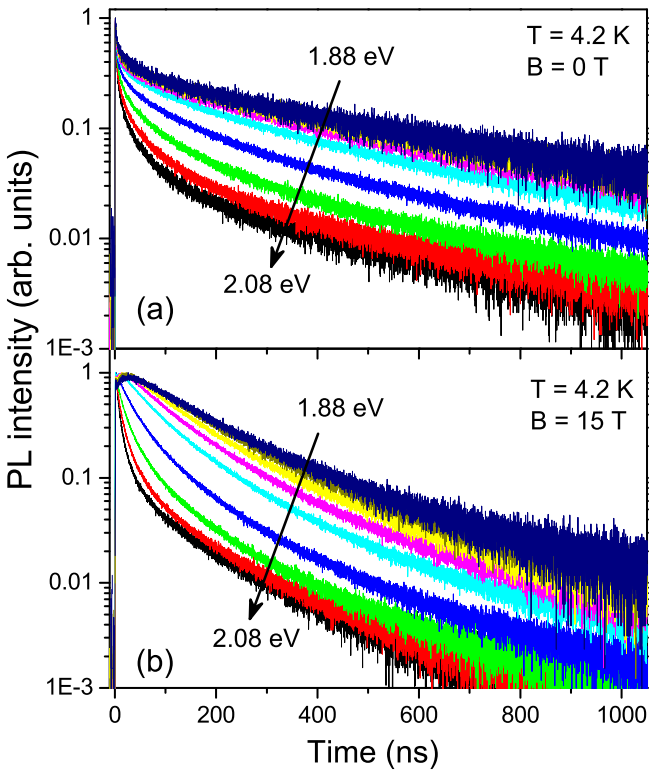

FIG. 5. (Color online) Spectrally resolved PL dynamics of the 3.4 nm CdTe NCs measured at (a) $B = 0$ T and (b) 15 T. The detection energy is varied in the range from 1.88 to 2.08 eV. The signals are normalized on their intensity at zero delay, i.e., right after the excitation pulse.

The spectrally resolved PL dynamics change considerably in an external magnetic field, compare Figs. 5(a) and 5(b). In a magnetic field the bright and dark exciton states become mixed, which results in the vanishing of the fast component and the shortening of the slow one. For example, the slow component of the PL decay at 2.08 eV (black line) shortens from 320 to 120 ns, when the magnetic field is increased to 15 T. Compared with the PL dynamics measured at the high energy side of the PL spectra, the PL decay measured at the low energy side shows a qualitatively different behavior. The PL dynamics at 1.88 eV (blue line) has a small initial rise and then decays, see Fig. 5(b). This rise can be explained only by the energy transfer process in which dark exciton states in larger NCs are fed by smaller NCs.

Further confirmation for the role of the energy transfer in the PL decay dynamics is shown in Fig. 6. Here the PL dynamics from two NC ensembles are measured in the magnetic field $B = 15$ T at the same energy of 1.88 eV, where the low energy tail of the 3.4 nm ensemble overlaps with the high energy tail of the 3.7 nm ensemble. Due to the NC size dispersion in the ensembles the specific energy corresponds to the specific NC size. While the PL dynamics differ drastically being strongly contributed by the energy transfer.

Figures 7(a)–7(c) show the PL dynamics measured at different magnetic fields for three energies on the 3.4 nm NCs, compare with Fig. 1. For clarity, Figs. 7(d)–7(f) are closeups of the initial 50 ns of the PL dynamics and show their amplitude on a linear scale. The PL decay at the high energy position

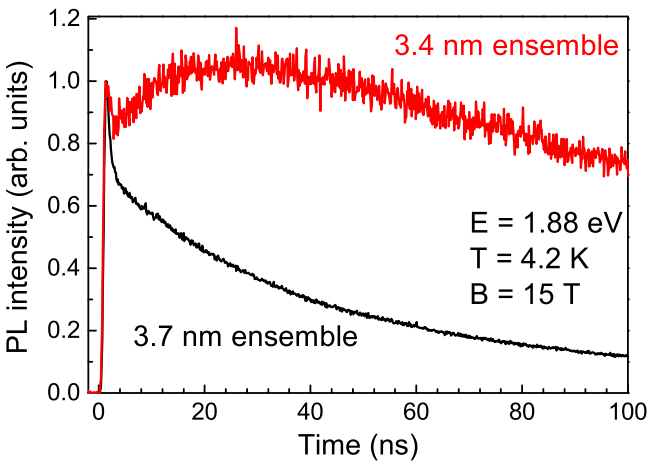

FIG. 6. (Color online) Spectrally resolved PL dynamics of the 3.4 and 3.7 nm CdTe NC ensembles measured at the energy of 1.88 eV, see Fig. 1(a).

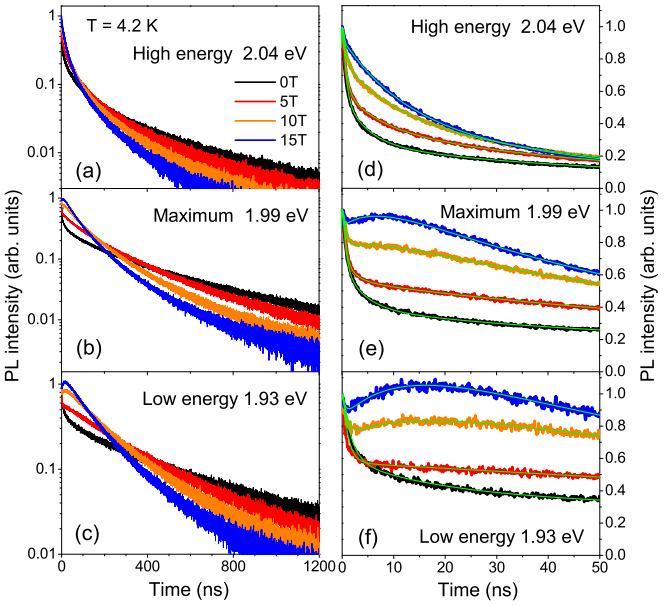

FIG. 7. (Color online) (a-c) PL dynamics of the 3.4 nm CdTe NCs measured at different spectral energies (see Fig. 1) and different magnetic fields. (d)–(f) The PL dynamics during the initial 50 ns. The green lines show fits to these curves with the function described in the Appendix.

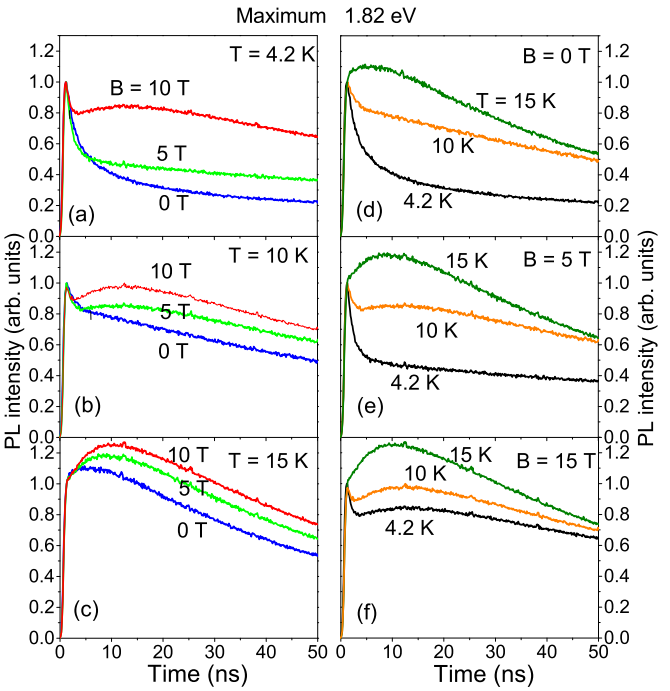

FIG. 8. (Color online) PL dynamics of the 3.7 nm CdTe NCs measured at the maximum of the PL band at 1.82 eV for various magnetic fields and temperatures.

shows the behavior typical for colloidal NCs, see Figs. 7(a) and 7(d). With increasing magnetic field, the fast component vanishes and the slow component shortens due to the mixing of bright and dark exciton states. However, a different behavior is observed at the maximum of PL spectra in Figs. 7(b) and 7(e). The PL dynamics at $B = 0$ T shows a decay in the time frame $t \in (5\,\text{ns}, 15\,\text{ns})$, which slows down with increasing magnetic field and turns into a rise at $B = 15$ T. Such unusual behavior is even more prominent at the low energy position, see Figs. 7(c) and 7(f). At $B = 15$ T the PL intensity at $t = 12$ ns is larger than the intensity at $t = 0$ ns.

A qualitatively very similar behavior was found for the 3.7 nm NCs, whose PL dynamics during the initial 50 ns measured at the PL maximum of 1.82 eV is presented in Fig. 8. In Figs. 8(a)–8(c) the PL dynamics measured at fixed temperature are compared for different magnetic fields. At $T = 4.2$ K the PL dynamics shows a decay at $B = 0$ T. At higher fields the PL intensity in the time interval $t \in (5\,\text{ns}, 15\,\text{ns})$ starts to grow, and at 15 T the decay turns into a rise. This behavior is more pronounced at higher temperatures, see Fig. 8(b). At 10 K, the decay turns to a rise already at $B = 5$ T. At even higher temperature of 15 K the fast decay component within the first 5 ns disappears, which can be seen in Figs. 8(a) and 8(b), and only a slow rise is visible during the initial 10 ns, see Fig. 8(c). The rise time increases for stronger magnetic fields.

Besides the magnetic field, the shape of the PL decay is also strongly influenced by temperature. As shown in Fig. 8(d), the PL dynamics at 4.2 and 10 K start with a fast decay component, while this fast component cannot be seen at 15 K. Instead, the PL dynamics starts with a rise of the PL intensity. At $B = 5$ T the rise of the PL intensity becomes more prominent, see Fig. 8(e). At $B = 15$ T the PL dynamics show this rise during the initial 15 ns at all studied temperatures. The fast decay component presents at 4.2 and 10 K, but disappears at 15 K, see Fig. 8(f).

Figure 9 shows the spectral dependence of the PL decay times of the 3.4 nm CdTe NCs for $B = 0$ and 15 T measured at $T = 4.2$ K. The PL decay times were obtained by fitting the spectrally resolved PL decays shown in Fig. 5 with the multiexponential function given by Eq. (A2) as described in the Appendix. In Fig. 9(a) the green triangles correspond to the fast component $\tau_{\text{ai}}^{\text{A}}$ observed at the very beginning of the PL decay. We relate this decay to the relaxation of excitons from the bright state to the dark state. The black closed diamonds correspond to the longest component $\tau_{\text{ai}}^{\text{F}}$, related to the decay of the dark excitons that are not involved in the energy transfer process as donors. The blue open triangles correspond to the component $\tau_{\text{d}}^{\text{F}}$ related to the dark excitons involved in the energy transfer process as donors having, therefore, a shortened lifetime. The amplitude of this component is small at the low energy side of the PL spectra, where the FRET does not contribute to the PL dynamics, and increases towards the high energy side of the PL spectra. The fast component marked by red circles, which appears only at the high energy side of the PL spectra, is most likely related to the energy transfer from the bright exciton states. One can see that at $B = 0$ T the characteristic times of all these components show no apparent spectral dependence, while their relative amplitudes are spectrally dependent.

For the PL dynamics at a magnetic field of 15 T the characteristic times are collected in Fig. 9(b). Here the open squares correspond to the rising component induced by the energy transfer. This component is visible only at the low energy side of the PL spectra. Compared with the zero-field case, two new components (the red stars and the orange circles)

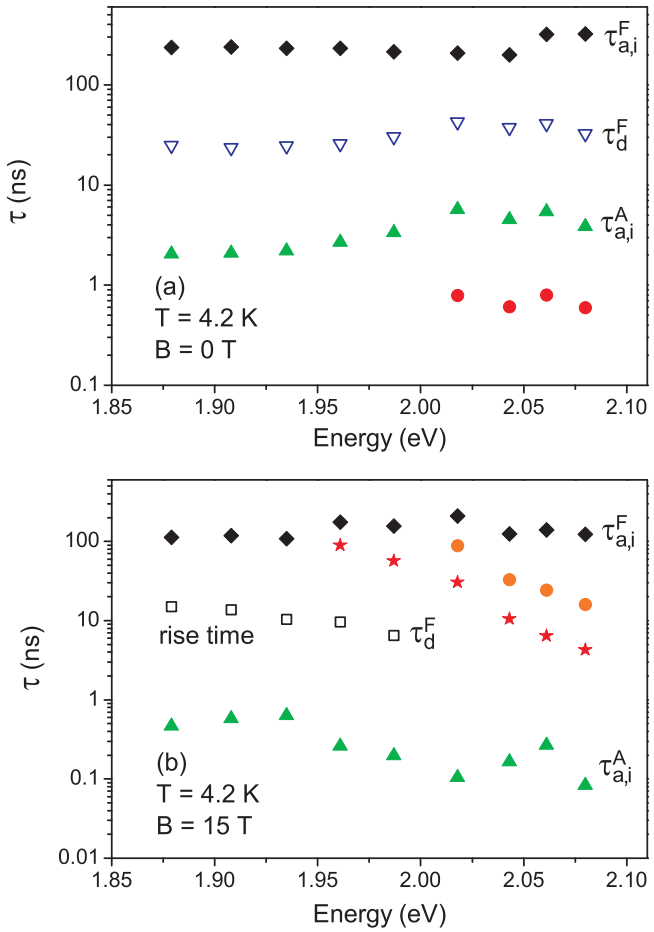

FIG. 9. (Color online) Spectral dependence of the PL decay and rise times of the 3.4 nm CdTe NCs for (a) $B = 0$ T and (b) 15 T at $T = 4.2$ K. The open squares in (b) show the rise time of the initial rising component that appears in magnetic field [see, e.g., the blue line in Fig. 7(f)]. The PL decay times are obtained by fitting the spectrally resolved PL decay shown in Fig. 5 with the multiexponential function of Eq. (A2) given in the Appendix.

appear at the high energy side of the PL spectra, indicating that new energy transfer paths are activated by the magnetic field or additional NCs become involved in the FRET. On the basis of these characteristic decay times, we developed a theoretical model describing the observed experimental results. Description of the model and presentation of the simulation results will be done in the following sections.

Figure 10 shows the magnetic field dependence of the characteristic times for the 3.4 nm CdTe NCs measured at the low energy side of the PL spectra at 1.93 eV for $T = 4.2$ K. The shortest component (green triangles) is related to the bright-dark relaxation time $\tau^A_{a,i}$. The longest component $\tau^F_{a,i}$ (black closed diamonds) corresponding to the dark exciton decay shortens by a factor of $\sim$2 with magnetic field increasing from 0 to 15 T. The component represented by the blue triangles has the same origin as that in Fig. 9(a), and is related to FRET. Its amplitude vanishes with increasing magnetic field. The open squares correspond to the component with negative amplitude in the fitting functions (see Appendix), that describes the rise in the PL dynamics of the acceptor NCs

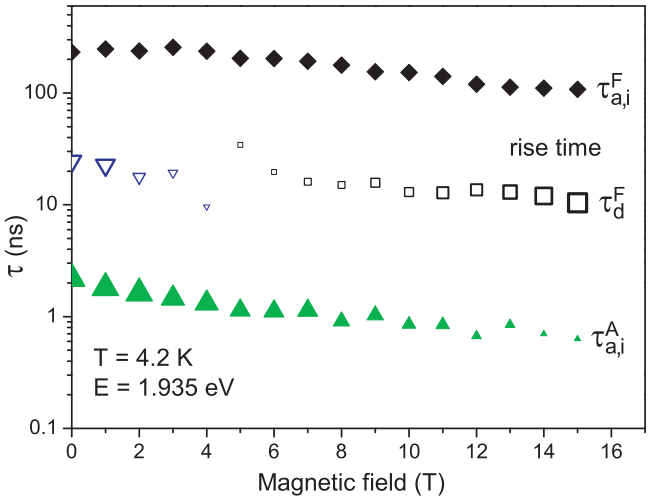

FIG. 10. (Color online) Magnetic field dependence of the PL decay and rise times of the 3.4 nm CdTe NCs measured at 1.93 eV. The size of symbols (except for the closed diamonds) is proportional to the amplitude of the corresponding component.

induced by the energy transfer. This rise time decreases from 34 ns at 0 T down to 10 ns at 15 T.

IV. THEORETICAL CONSIDERATIONS

In this section we present the theoretical model that describes the PL intensity of an ensemble of NCs taking into account the energy transfer process between them. We start from the general assumptions about the properties of the NC ensemble and consider the donor and the acceptor NCs participating in the energy transfer process as well as the independent NCs (not participating in the FRET process). We discuss the possible recombination, relaxation, and energy transfer pathways for excitons and write down a system of rate equations for the exciton populations in donor, acceptor, and independent NCs.

A. General assumptions

For the sake of clarity, let us consider an ensemble of closely packed prolate CdTe NCs with the ground exciton state split into the bright (optically allowed A exciton with spin projection ± 1 on the anisotropy axis) and the dark (optically forbidden F exciton with spin projection ± 2) exciton states. Since the probability of the Förster energy transfer decreases proportional to R_{da}^{-6}, where R_{da} is the distance between the centers of the donor and acceptor NCs, it is the largest for the nearest neighbor NC pairs and already much smaller for the next nearest neighbors. Thus, in the model we consider the energy transfer process only between the nearest neighbors. In this case the energy transfer rate is determined by the magnitude of exciton dipole moments in the donor and acceptor NCs and by the overlap integral between the donor emission and acceptor absorption spectra, while the average distance can be estimated as the mean size of the NCs: $R_{da} \approx d$. We consider the low excitation regime, which is defined by assuming that the portion of initially excited NCs at each energy $[N_0(E)]$ within the NC ensemble

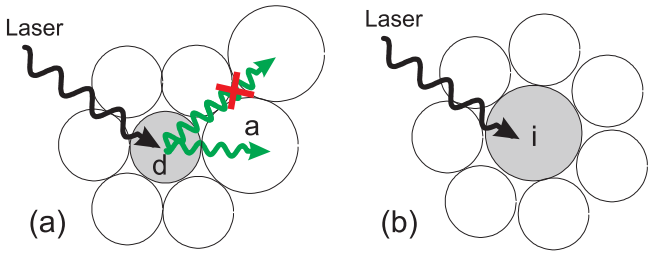

FIG. 11. (Color online) Scheme of possible processes initiated by optical excitation in a NC ensemble: (a) Energy transfer between the nearest donor and acceptor NCs and (b) independent NCs for which no energy transfer occurs.

is negligible. This allows us to consider the energy transfer only to initially unexcited NCs. In turn, initially excited NCs with the ground state exciton energy E may act as donors [with probability $f_d(E)$] and transfer their excitation to the nearest acceptor NCs [see Fig. 11(a)], or as independent NCs which do not participate in the energy transfer process [see Fig. 11(b)]. Thus, the total number of initially excited donor and independent NCs is $N_d^0(E) = N_0(E) f_d(E)$ and $N_i^0(E) = N_0(E)[1 - f_d(E)]$, respectively. The properties of the energy-dependent probability function $f_d(E)$ will be discussed later. Also, we neglect all cascade processes, so that one NC cannot act as donor and acceptor simultaneously.

After these general remarks on the assumptions related to the ensemble of NCs, let us consider the energy transfer mechanism between the donor and acceptor NCs in more detail. Let us consider a NC with the ground state exciton energy E_a at the low energy side of the PL band arising from the acceptors. A smaller NC with higher ground state exciton energy $E_d = E_a + E_{da}$ may play the role of a donor for the chosen acceptor if there is a nonzero overlap between the donor emission spectrum and the acceptor absorption spectrum. We assume for simplicity that for each E_d there is only one excited level $E_a + E_{da}$ in the nearest acceptor NCs and consider the energy difference E_{da} as a parameter in our model.

In case of initial nonresonant excitation with the rate G using photon energies well above the ground exciton state energy the relaxation of the hot excitons to the ground state is a fast process assisted by optical phonons and the interaction with the surface [52]. After relaxation of the exciton to the ground state it can be resonantly transferred to another (acceptor) NC. The energy transfer process between the donor NC with ground state exciton energy E_d and the acceptor NC with ground state exciton energy E_a is shown schematically in Fig. 12. We assume that the bright (optically allowed A) and dark (optically forbidden F) exciton states have approximately the same energy splitting ΔE_{AF} in the donor and acceptor NCs. The energy transfer process consists of two steps. Initially the resonant transfer from the ground energy state of the donor NC to the first excited energy state of the acceptor NC takes place. We assume that the bright and dark ground exciton states in the donor NC are in resonance with the first excited bright and dark states in the acceptor NC, respectively. After the energy transfer, fast energy relaxation from the excited to the ground state of the acceptor NC occurs. This relaxation process may occur in two different ways, either spin conserving and thus

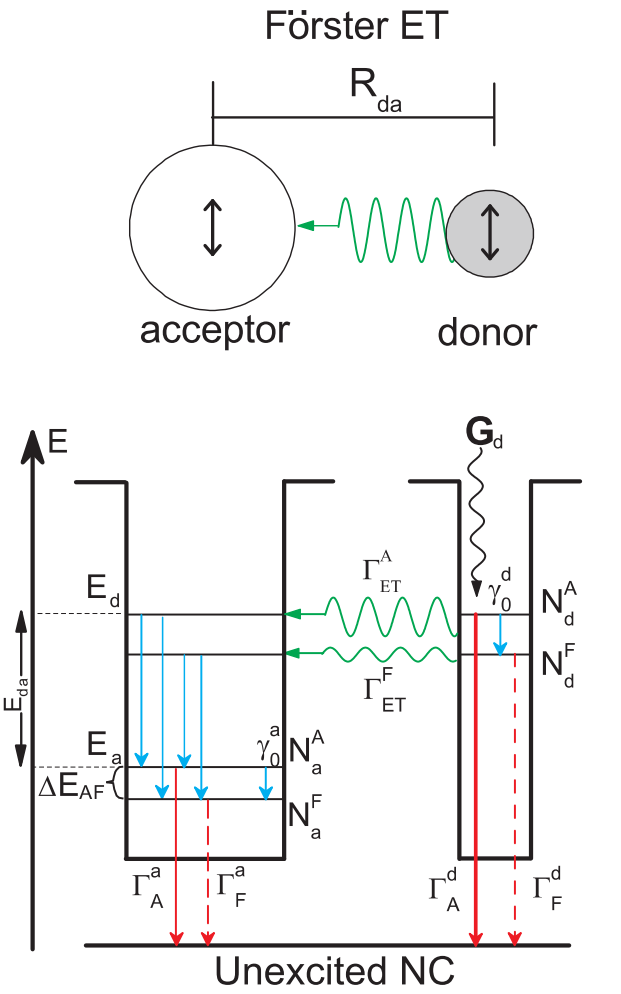

FIG. 12. (Color online) Schematic of the energy transfer process between a donor NC with energy E_d and an acceptor NC with energy E_a. The energy transfer is shown by the green arrows, the relaxation processes by the blue arrows, the recombination pathes by the red arrows, and the laser pumping by the black arrow.

allowing relaxation only from the bright to the bright states or from the dark to the dark state or spin nonconserving. For the sake of clarity, we assume here the energy difference E_{da} to be large enough for the fast nonconserving relaxation processes, similar to those taking place after the initial excitation of all NCs. In this case the relaxation from the bright and dark excited states occurs with equal probability to the ground bright and dark states without any "memory" effects. However, the model can be easily modified for the case of spin conserving relaxation in the acceptor NCs.

B. Rate equations for the bright and dark exciton populations

To be able to describe the experimental data with our model we express the PL intensity in terms of exciton populations in the NCs. The total population of excitons $N(E,t)$ with a given ground state exciton energy E can be written as the sum of exciton populations in the donor NCs N_d, the independent NCs N_i, and the acceptor NCs N_a, NCs. In turn, the population of excitons in each type of NCs consists of the populations of

excitons in the bright $N^{\rm A}_{\rm d,i,a}$ and dark $N^{\rm F}_{\rm d,i,a}$ states:

$$N(E,t) = N_{\rm i}(E,t) + N_{\rm d}(E,t) + N_{\rm a}(E,t), \tag{3}$$

$$N_{\rm d,i,a}(E,t) = N^{\rm A}_{\rm d,i,a}(E,t) + N^{\rm F}_{\rm d,i,a}(E,t). \tag{4}$$

Using the populations of the bright and dark excitons in each type of NCs, one obtains for the PL intensity of a NC ensemble at a given exciton energy E,

$$I(E,t) = I_{\rm i}(E,t) + I_{\rm d}(E,t) + I_{\rm a}(E,t), \tag{5}$$

$$I_{\rm d,i,a}(E,t) = \Gamma^{\rm rad}_{\rm A}(E) N^{\rm A}_{\rm d,i,a}(E,t) + \Gamma^{\rm rad}_{\rm F}(E) N^{\rm F}_{\rm d,i,a}(E,t). \tag{6}$$

Here $\Gamma^{\rm rad}_{\rm A,F}$ are the radiative recombination rates. Thus, knowing the time evolution of the populations $N^{\rm A,F}_{\rm d,i,a}(E,t)$, one can fully describe the time evolution of the PL intensity from a NC ensemble.

The pair of the bright-dark exciton rate equations for the donor and the independent NCs can, according to Fig. 12, be written as

$$\frac{dN^{\rm A}_{\rm d,i}(E,t)}{dt} = -N^{\rm A}_{\rm d,i}\left(\Gamma_{\rm A} + \gamma_0 + \gamma_{\rm th} + \Gamma^{\rm A}_{\rm ET}\right) + N^{\rm F}_{\rm d,i}\gamma_{\rm th} + \frac{1}{2}G_{\rm d}(E,t), \tag{7}$$

$$\frac{dN^{\rm F}_{\rm d,i}(t)}{dt} = -N^{\rm F}_{\rm d,i}(t)\left(\Gamma_{\rm F} + \gamma_{\rm th} + \Gamma^{\rm F}_{\rm ET}\right) + N^{\rm A}_{\rm d,i}(t)(\gamma_0 + \gamma_{\rm th}) + \frac{1}{2}G_{\rm i}(E,t). \tag{8}$$

Here the recombination rates $\Gamma_{\rm A,F} = \Gamma^{\rm d}_{\rm A,F}$ (which may include both radiative and nonradiative paths other than the energy transfer), as well as the relaxation rates $\gamma_0 = \gamma^{\rm d}_0$ and $\gamma_{\rm th} = \gamma^{\rm d}_{\rm th}$ (thermally induced relaxation given for the case of a one-phonon process by $\gamma_{\rm th} = \gamma_0/[\exp(\Delta E_{\rm AF}/k_{\rm B}T) - 1]$) should be taken at the exciton energy $E_{\rm d}$. The energy transfer rates are denoted as $\Gamma^{\rm A}_{\rm ET}$ and $\Gamma^{\rm F}_{\rm ET}$ for the bright and dark exciton states in the donor NCs, respectively, and have to be set to zero in the independent NCs. The rates of pumping of the bright and dark exciton states are denoted as $\frac{1}{2}G_{\rm d,i}(E,t)$ and are equal because of the spin nonconserving relaxation of the hot excitons, as mentioned previously.

The rate equations for the acceptor NCs, according to Fig. 12, can be written as

$$\frac{dN^{\rm A}_{\rm a}(E,t)}{dt} = -N^{\rm A}_{\rm a}(\Gamma_{\rm A} + \gamma_0 + \gamma_{\rm th}) + N^{\rm F}_{\rm a}\gamma_{\rm th} + \frac{1}{2}\left(N^{\rm A}_{\rm d}\Gamma^{\rm A}_{\rm ET} + N^{\rm F}_{\rm d}\Gamma^{\rm F}_{\rm ET}\right), \tag{9}$$

$$\frac{dN^{\rm F}_{\rm a}(E,t)}{dt} = -N^{\rm F}_{\rm a}(\Gamma_{\rm F} + \gamma_{\rm th}) + N^{\rm A}_{\rm a}(\gamma_0 + \gamma_{\rm th}) + \frac{1}{2}\left(N^{\rm A}_{\rm d}\Gamma^{\rm A}_{\rm ET} + N^{\rm F}_{\rm d}\Gamma^{\rm F}_{\rm ET}\right). \tag{10}$$

Here the population $N_{\rm a}$ should be considered at the exciton energy $E_{\rm a}$ (as well as the recombination rates $\Gamma_{\rm A,F} = \Gamma^{\rm a}_{\rm A,F}$ and the relaxation rates $\gamma_0 = \gamma^{\rm a}_0$ as well as $\gamma_{\rm th} = \gamma^{\rm a}_{\rm th}$ rates), while the population $N_{\rm d}$ has to be taken at the energy $E_{\rm a} + E_{\rm da}$. Since we consider the low excitation regime, a pumping term is not included in the rate equations for the acceptor NCs.

V. MODELING OF THE EXPERIMENTAL DATA

A. Determination of decay times for donor, acceptor, and independent NCs

The system of rate equations described in Sec. IV B can be solved numerically or analytically. The analytical solution can be simplified in the low temperature limit, assuming $\gamma^{\rm a(d)}_{\rm th} \approx 0$. Additionally, we consider the following hierarchy of rates $\gamma_0 \gg \Gamma_{\rm A} \gg \Gamma_{\rm F}$ and also assume that all rates do not depend on energy. This allows us to obtain simple approximate expressions for the time evolution of the populations $N^{\rm A,F}_{\rm d,i,a}(E,t)$, which depend on the energy E only via the energy dependent initial conditions $N^{\rm A,F}_{\rm d,i,a}(E,t=0)$. These solutions can be written for donor NCs and independent NCs as

$$N^{\rm A}_{\rm d,i}(E,t) = N^{\rm A}_{\rm d,i}(E,t=0)\exp\left(-t/\tau^{\rm A}_{\rm d,i}\right), \tag{11}$$

$$N^{\rm F}_{\rm d,i}(E,t) \approx -N^{\rm A}_{\rm d,i}(E,t) + N^{0}_{\rm d,i}(E)\exp\left(-t/\tau^{\rm F}_{\rm d,i}\right), \tag{12}$$

and for the acceptor NCs as

$$N^{\rm A}_{\rm a}(E,t) \approx N^{\rm A}_{\rm d}(E+E_{\rm da},t=0) \times\left[\exp\left(-t/\tau^{\rm A}_{\rm a}\right) - \exp\left(-t/\tau^{\rm A}_{\rm d}\right)\right], \tag{13}$$

$$N^{\rm F}_{\rm a}(E,t) = -N^{\rm A}_{\rm a}(E,t) + N^{0}_{\rm d}(E+E_{\rm da}) \times\left[\exp\left(-t/\tau^{\rm F}_{\rm a}\right) - \exp\left(-t/\tau^{\rm F}_{\rm d}\right)\right]. \tag{14}$$

Here we use $N^{0}_{\rm d,i}(E) = N^{\rm A}_{\rm d,i}(E,t=0) + N^{\rm F}_{\rm d,i}(E,t=0)$ and $N^{0}_{\rm a}(E) = N^{\rm A}_{\rm a}(E,t=0) + N^{\rm F}_{\rm a}(E,t=0) = 0$. The characteristic times are

$$\frac{1}{\tau^{\rm A}_{\rm d}} = \Gamma_{\rm A} + \gamma_0 + \Gamma^{\rm A}_{\rm ET}, \tag{15}$$

$$\frac{1}{\tau^{\rm F}_{\rm d}} = \Gamma_{\rm F} + \Gamma^{\rm F}_{\rm ET}, \tag{16}$$

$$\frac{1}{\tau^{\rm A}_{\rm a,i}} = \Gamma_{\rm A} + \gamma_0, \tag{17}$$

$$\frac{1}{\tau^{\rm F}_{\rm a,i}} = \Gamma_{\rm F}. \tag{18}$$

The equations allow us to reveal the decay times for each kind of NCs. By comparing these times with the times extracted from the multiexponential fit of the experimental decay curves we evaluate the rates $\Gamma_{\rm F,A}$, $\Gamma^{\rm F,A}_{\rm ET}$, and γ_0. We assume that the recombination rate of the dark exciton $\Gamma_{\rm F}$ and its magnetic field dependence can be directly associated with the longest decay component $\Gamma_{\rm F} = 1/\tau^{\rm F}_{\rm a,i}$ obtained by fitting the experimental decay curves and shown by the black diamonds in Figs. 9 and 10. One sees that this rate indeed very weakly depends on the energy but increases nearly by a factor of 2 with increasing magnetic field up to 15 T. This increase is caused by the fact that despite the cubic symmetry of the CdTe crystal lattice, the NCs possess an anisotropic axis related to their nonspherical shape [50]. As a result, a magnetic field having

TABLE II. Magnetic-field dependent parameters determined from the analysis of the multiexponential fit and from the simulation of the PL dynamics with the rate equations. Γ_{ET}^{F} is the energy transfer rate from the dark exciton state, Γ_F is the recombination rate of the dark exciton state, and γ_0 is the relaxation rate from the bright to the dark exciton states at $T = 0$ K (taken to be the same for all donor and acceptor NCs). The parameter w is the fraction of bright excitons in independent NCs at time $t = 0$.

		Multiexponential fit		Rate equations		
B (T)	γ_0 (ns^{-1})	Γ_F (ns^{-1})	Γ_{ET}^{F} (ns^{-1})	Γ_F (ns^{-1})	Γ_{ET}^{F} (ns^{-1})	w
0	0.45	0.004		0.0035	0.055	0.23
5	0.72	0.005	0.023	0.0040	0.055	0.17
10	1.0	0.007	0.069	0.0065	0.070	0.13
15	1.3	0.009	0.090	0.0085	0.090	0.11

nonzero projection on the anisotropy axis mixes the bright and dark exciton states similar to the well known situation in hexagonal CdSe NCs [17].

Furthermore, the bright exciton recombination rate $\Gamma_A = 0.1$ ns^{-1} and the value of the bright-dark splitting $\Delta E_{AF} = 2.2$ meV are obtained from the temperature dependence of the PL decay (not shown here) [48]. We determine the relaxation rate γ_0 and its magnetic field dependence from the bright exciton lifetime $\tau_{a,i}^{A}$ at $E_a = 1.93$ eV (the green triangles in Fig. 10) as $\gamma_0 = 1/\tau_{a,i}^{A} - \Gamma_A$. The energy transfer rate Γ_{ET}^{F} can be found from the difference of the dark exciton lifetimes $\Gamma_{ET}^{F} = 1/\tau_d^F - 1/\tau_{a,i}^{F}$. However, attempts to estimate this rate from the decay components at the high energy (donor) side of the spectrum are complicated by the fact that there are more components than just one in high magnetic field and their rates depend on the spectral position, see Fig. 9(b). For this reason we use the rise rates [the open squares in Figs. 10 and 9(b)] observed at the low energy side of the spectrum at $B \geqslant 4$ T in order to estimate τ_d^F averaged over the spectral position and to obtain the magnetic field dependence of the Γ_{ET}^{F}. The determination of the energy transfer rate Γ_{ET}^{A} from the bright exciton is more difficult because of its short lifetime. We estimate that the energy transfer from the bright exciton state is faster than the relaxation to the dark exciton state in the donor NCs. The parameters determined from the analysis of the multiexponential fit for magnetic fields of $B = 0$, 5, 10, and 15 T are summarized in Table II.

B. Shift of the cw PL spectrum due to the nonradiative energy transfer

The PL spectrum measured at time $t = 0$ can be approximated by a Gaussian form with a peak energy at $E = E_0$:

$$I(E,t=0) = \frac{I}{\sigma\sqrt{2\pi}} \exp\left[-\frac{(E-E_0)^2}{2\sigma^2}\right], \tag{19}$$

where I is the total spectrally integrated intensity at $t = 0$ and σ corresponds to the linewidth at half-maximum according to $2\sigma\sqrt{2\ln 2}$. Neglecting the spectral dispersion of the recombination rates of the bright and the dark excitons Γ_A and Γ_F as well as their relative populations at $t = 0$, we assume that the shape of the time-resolved PL spectrum at $t = 0$ reflects the initial energy dispersion of the excitons populations: $I(E,t=0) \propto N^0(E)$.

To simulate the temporal shift of the cw PL peak position compared to the peak position at time $t = 0$ we solve the system of rate equations in the steady-state regime. Considering the low temperature limit and constant generation rates $G_{d,i} = GN_{d,i}^{0}(E)$ we obtain the following solutions for the populations in the different kinds of NCs:

$$N_{d,i}^{A}(E) = \frac{1}{2} G\tau_{d,i}^{A} N_{d,i}^{0}(E), \tag{20}$$

$$N_{d,i}^{F}(E) = \frac{\tau_{d,i}^{F}}{2}\left[GN_{d,i}^{0}(E) + \gamma_0 N_{d,i}^{A}(E)\right], \tag{21}$$

$$N_a^A(E) = \frac{\tau_a^A}{2}\left[\Gamma_{ET}^{A} N_d^A(E_d) + \Gamma_{ET}^{F} N_d^F(E_d)\right], \tag{22}$$

$$N_a^F(E) \approx 2N_a^A(E)\frac{\tau_a^F}{\tau_a^A}, \tag{23}$$

where $E_d = E + E_{da}$. The final equation describing the cw spectrum is rather cumbersome but can be simplified by taking into account the ratio of bright and dark exciton lifetimes. From Eqs. (20)–(23) one can see that the populations of the bright and dark excitons are proportional to their characteristic lifetimes. As the lifetime of the dark excitons is two orders of magnitude longer than the bright exciton lifetime we can neglect the contribution of the bright excitons. In this case a simple equation for the shift of the cw spectrum can be obtained:

$$I_{PL}^{cw}(E) = I(E,t=0)[1 - K_{ET}T_d(E)], \tag{24}$$

$$T_d(E) = f_d(E) - f_d(E+E_{da})\frac{N_0(E+E_{da})}{N_0(E)}, \tag{25}$$

where

$$K_{ET} = \frac{\Gamma_{ET}^{F}}{\Gamma_{ET}^{F} + \Gamma_F} \tag{26}$$

describes the efficiency of the energy transfer process from the dark exciton state. The physical meaning of the transfer function T_d is clearly seen: the excitation is transferred from the spectral region $T_d(E) > 0$ to the region where $T_d(E) < 0$.

We choose for the function $f_d(E)$ a Gaussian form with the peak at $E_0 + E_{da}$. To keep the energy distance E_{da} at the same (average) value over the spectrum, we allow the dispersion σ_d of the $f_d(E)$ to be larger than σ. Comparison of the cw spectrum with the time-resolved spectrum at $t = 0$ allows us to determine the dispersion $\sigma_d = 90$ meV and the average value of $E_{da} = 106$ meV. The comparison of the exact solution with the solution given by Eq. (24) shows no difference. Physical meaning is that the fast relaxation of excitons from the bright state with the rate γ_0 results in the accumulation of excitons in the dark state. In case of the cw excitation this is equivalent to the direct generation of dark excitons only.

In the absence of the bright excitons in the donor NCs the shift of the PL peak in the cw regime is determined by the energy transfer efficiency K_{ET} from the dark excitons. For modeling the spectral shift in Fig. 13(a) we used $K_{ET} \approx 0.9$ determined for $B = 15$ T with the rates given in Table II.

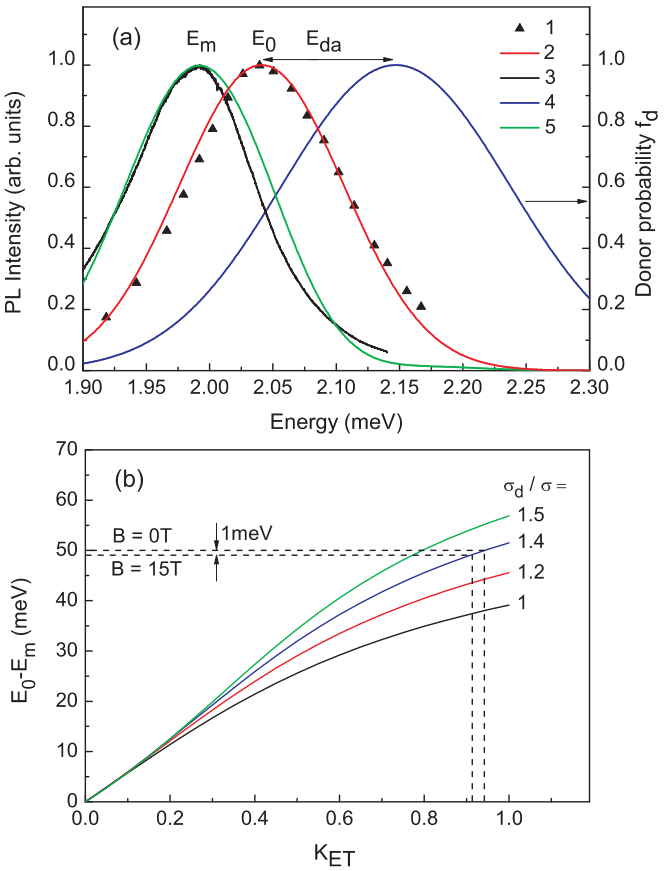

FIG. 13. (Color online) (a) Modeling of the PL spectra: (1) Experimentally measured time-resolved PL spectrum of the 3.4 nm NCs at $t = 0$. (2) Gaussian-shaped time-resolved PL spectrum $I(E,t = 0)$ with the peak at E_0. (3) Experimentally measured cw PL spectrum with the peak at E_m. (4) Donor probability function f_d. (5) Modeled cw PL spectrum given by the solution of the rate equations in the steady-state regime. (b) Modeled dependence of the PL shift maximum $E_0 - E_m$ on the energy transfer efficiency K_{ET}.

Figure 13(b) shows the dependencies of the PL maximum shift $E_0 - E_m$ on the ET efficiency K_{ET} for different values of the ratio σ_d/σ. One sees that in the range of large K_{ET} close to unity, the PL maximum shift $E_0 - E_m$ changes insignificantly. We remind also that the experimentally measured unpolarized cw spectra in different magnetic fields differ insignificantly as well [compare, for example, the cw spectra for $B = 0$ (the black line) and $B = 15$ T (the red line) in Fig. 1(a)]. The nonlinear dependence of $E_0 - E_m$ on K_{ET} can be obtained from Eq. (24) as

$$E_0 - E_m = \Delta(E_m) K_{ET}, \tag{27}$$

$$\Delta(E) = \frac{\sigma^2}{N_0(E)} \frac{\partial[N_0(E) T_d(E)]}{\partial E}. \tag{28}$$

Note that the recombination rate Γ_F in Eq. (26) may include also the nonradiative decay path other than the energy transfer. The presence of fast nonradiative recombination could prevent the observation of the spectral shift of the PL line caused by the energy transfer due to decrease of the K_{ET} value. It is not the case for the studied samples, where K_{ET} very close to unity is evaluated. To simplify the following modeling of the recombination dynamics we neglect the nonradiative mechanisms other than ET and assume hereafter the recombination rates to be purely radiative: $\Gamma_{A,F} = \Gamma^{rad}_{A,F}$.

C. Spectral dependence of the recombination dynamics

To simulate the recombination dynamics of the NC ensemble, we combine the solution of the system of rate equations for a donor-acceptor NC pair in the transient regime with the determined probability function $f_d(E)$ for the energy transfer. However, the initial conditions at $t = 0$ for the bright excitons $N^A_{d,i}(E,t = 0)$ and the dark excitons $N^F_{d,i}(E,t = 0)$ should be determined first. The relative populations of the bright and the dark excitons $N^A_{d,i}(E,t = 0)$ and $N^F_{d,i}(E,t = 0)$ and their corresponding contributions to the PL may depend on the conditions of excitation and detection. For photoexcitation with short laser pulses, the relaxation, recombination, and energy transfer processes start simultaneously. For our simulations at all energies, we choose as the initial time $t = 0$ the time when the initial growth of the PL intensity after the pumping pulse turns into a decay. Even if the exciton relaxation to the ground state occurs with an equal probability to the dark and bright states, their populations at $t = 0$ might be not equal. The reason is that the pulse duration (see Appendix) is comparable with the relaxation time between the bright and dark exciton states and with the energy transfer rate from the bright excitons. Hence, we introduce the initial condition for the bright exciton population in the independent NCs as $N^A_i(E,t = 0) = wN^0_i(E)$ and consider w as an energy independent parameter. The additional growth of the PL intensity after $t = 0$ is observed at the low energy side of the spectrum at 4.2 K only, with the rate corresponding to the energy transfer from the dark exciton [see Figs. 7(e), 7(f), 9(b), and 10]. For this reason we neglect in our simulation the energy transfer from the bright exciton states and use the initial condition for the donor NCs $N^A_d(E,t = 0) = 0$.

Using these initial conditions, a consistent modeling of the PL decay $I(E,t)$ for NCs with emission energies at $E = E_d = 2.04$ eV and $E = E_a = 1.93$ eV can be achieved. This modeling allows us to refine the values of the rates Γ_F and Γ^F_{ET} by comparing the simulated decay curves with the experimental data measured at $T = 4.2$ K for magnetic fields $B = 0$–15 T at the emission energies $E_a = 1.93$ eV and $E_d = 2.04$ eV, see Figs. 7(d) and 7(f). The refined parameters used in the modeling are listed in Table II. The results of the calculations are presented in Fig. 14. One sees that a good agreement with the experimental data is achieved for the PL decay of the NCs at E_a (see the red curves). For the PL decay at E_d (blue curves) the difference between the simulated and the experimental decay curves increases with the increasing magnetic field. Apparently this difference is caused by neglected additional nonradiative processes (for example, additional energy transfer to NCs other than those emitting at $E_a = 1.93$ eV), which are indicated by the additional decay times shown in Fig. 9(b) for the high energy emission of the PL in a magnetic field of $B = 15$ T. Accounting for the additional process with a decay rate of 0.035 ns^{-1} corresponding to the orange circles in Fig. 9(b) for the NCs at $E_d = 2.04$ eV allows us to simulate the decay curves [see the green curve in Fig. 14(d)] with better accuracy.

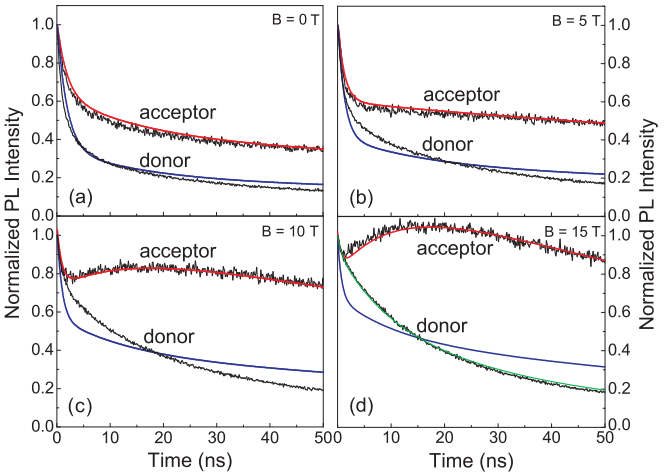

FIG. 14. (Color online) Experimental data (the black curves) and calculations of the PL dynamics of acceptor NCs at $E_a = 1.93$ eV (the red curves) and donor NCs at $E_a = 2.04$ eV (the blue curves) at $T = 4.2$ K for $B = 0$, 5, 10, and 15 T. The calculation results were achieved from solution of the rate equations Eqs. (8) and (10) using the parameters listed in Table II. The green curve for $B = 15$ T corresponds to the solution of the rate equations with an additional nonradiative process (see the description in text).

Using the refined parameters for the recombination and energy transfer rates we can also simulate the PL dynamics of the acceptor NCs at different temperatures. The calculations results at energy $E = E_a = 1.93$ eV for magnetic fields of $B = 0$, 10, and 15 T are shown in Fig. 15. The effect of the temperature is due to the increase of the bright exciton state population with increasing temperature.

Constructing the time-dependent intensities $I(E,t)$ obtained from Eq. (5) using the solutions of the rate equations in the time-resolved regime for all energies E, it is possible to model the time evolution of the spectrum as a whole and to describe the time evolution of the PL maximum $E(t)$. Using the approximate analytical solutions given by Eqs. (12) and (14) and neglecting the initial population of the bright excitons in the donor NCs we obtain the following expression:

$$E_0 - E(t) = \Delta[E(t)][1 - \exp(-t\Gamma_{ET}^{F})], \qquad (29)$$

where $\Delta[E(t)]$ given by Eq. (28) depends on energy and thus on time. In Eq. (2) used for fitting the experimentally observed temporal shift $E(t)$ in Fig. 4, two energy shifts $\Delta E_{1,2}$ and two characteristic shift rates $\Gamma_{\Delta E_{1,2}}$ were used. It is clear from Eq. (29) that the time evolution of the PL maximum cannot be described by a single exponential function even for the case when only one type of the energy transfer takes place. We can associate the slow component $\Gamma_{\Delta E_2}$ used in the fit in Fig. 4 according to Eq. (2) with the energy transfer rate from the dark exciton Γ_{ET}^{F}. The fast component $\Gamma_{\Delta E_1}$ is most probably caused by the energy dependence of the relaxation rate from the bright to the dark exciton states γ_0 or by the energy transfer from the bright exciton state that is neglected in our simulations.

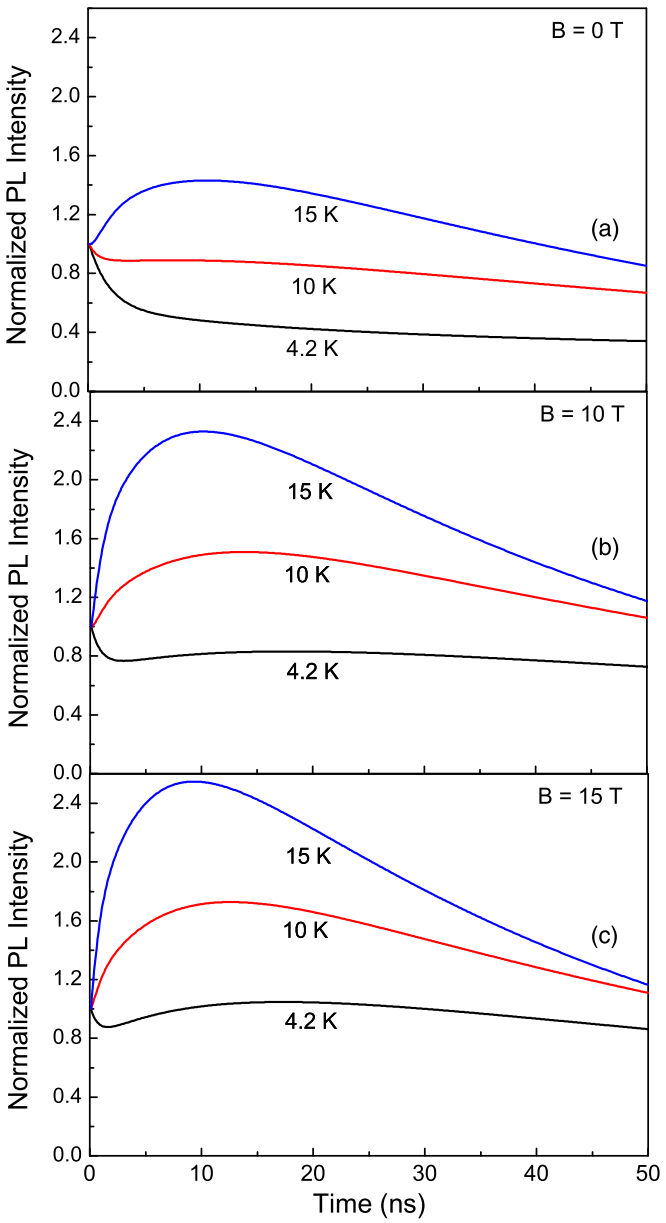

FIG. 15. (Color online) Modeling of the PL dynamics of the 3.4 nm NCs at energy $E = E_a = 1.93$ eV for the temperatures $T = 4.2$ K (the black curves), 10 K (the red curves), and 15 K (the blue curves) in magnetic fields of $B = 0$ (a), 10 T (b), and 15 T (c). The parameters used for the modeling are given in text and in Table II.

VI. DISCUSSION AND CONCLUSIONS

From the time-resolved PL data it is clearly seen that the typical time scales during which the energy shift of the PL maximum and the growth of the PL intensity at the low energy part of the spectrum take place are significantly longer than the lifetime of the bright excitons. This fact points to the important role of the dark exciton, but does not provide any insight on the underlying mechanisms. According to the experimental data and modeling results the reason for the prominent role of the dark exciton in the ET process is that the initial optical pumping is accompanied by the relaxation process from the bright to the dark state and by the fast energy transfer process from the

bright state. As a result, when we start observation at the certain conditional moment $t = 0$, the populations of the dark and bright excitons are already redistributed and the bright exciton is nearly depopulated in the donor NCs at low temperatures.

As mentioned above, the FRET occurs via dipole-dipole interaction. Therefore, the efficiency of FRET depends on the oscillator strength of the dipoles. In colloidal NCs the dark exciton state is not completely dark—it has some finite dipole moment and participates in the radiative recombination even at zero magnetic field due to the admixture of the bright exciton state [44]. The same admixture allows the dipole-dipole energy transfer from or to the dark exciton state in a zero magnetic field. An external magnetic field mixes additionally the bright and the dark exciton states, thus increasing the dipole moment μ of the dark exciton and its radiative rate [17]. This additional admixture leads to the enhancement of the energy transfer rate from the dark exciton state.

The enhancement of the energy transfer by the magnetic field can be seen already from Fig. 4(b). The shift of the peak position during the first 70 ns at $B = 15$ T (51 meV) is larger than that at 0 T (40 meV). Since the shift of the peak position is related to the energy transfer, we can conclude that the energy transfer is enhanced by the magnetic field. The importance of the energy transfer from the dark exciton state and its acceleration in the magnetic field is directly demonstrated by the simulation of the PL decay curves for a pair of donor-acceptor NCs. By adjusting the rates of excitons for a better matching of the simulated decay curves with the experimental dependencies of these rates on magnetic field, refined rates were achieved.

In Fig. 16 the dependencies of the recombination rate Γ_F and the ET rate Γ_{ET}^F on magnetic field are presented. The black circles show the rates obtained directly from the multiexponential fitting and the red circles give the rates obtained from fitting the experimental PL decays with the solution of the rate equations. One sees that the recombination rates obtained by both methods almost coincide. From the results of the modeling a significant correction to magnetic field dependence of the Γ_{ET}^F rate [red triangles versus black triangles in Fig. 16(b)] in low magnetic fields is obtained. According to the modeling of the PL decays of donor and acceptor NCs, the ET rate is constant in magnetic fields up to 6 T [the red triangles in Fig. 16(b)]. The magnetic field dependencies of the normalized rates are fitted by $\Gamma_F(B)/\Gamma_F(0) = 1 + (B/12)^2$ and $\Gamma_{ET}^F(B)/\Gamma_{ET}^F(0) = 1 + (B/12)^2 + (B/24)^4$. The B^2 dependence for the dark exciton recombination rate corresponds to the linear in B increase of the dark exciton dipole moment $\mu \propto B$, caused by the magnetic-field-induced admixture of the bright exciton, so that $\Delta\Gamma_F \propto \mu^2 \propto B^2$. When the FRET occurs from the dark to the bright exciton state, its rate will be enhanced by the magnetic field according to Eq. (1) as $\propto \mu_d^2 \propto B^2$. In the case of FRET between two dark exciton states, its rate will be enhanced by the magnetic field according to Eq. (1) as $\propto \mu_d^2 \mu_a^4 \propto B^4$. Therefore, the B^2 and B^4 dependencies for the energy transfer rate show that the energy transfer from the dark exciton state in the donor NC may take place to both bright and dark exciton states in the acceptor NC.

The rate of the energy transfer from the dark exciton state $\Gamma_{ET}^F(B)$ is enhanced in the magnetic field. This enhancement is evidenced in the time-resolved studies of the PL dynamics and the time evolution of the PL maximum in the ensemble [see

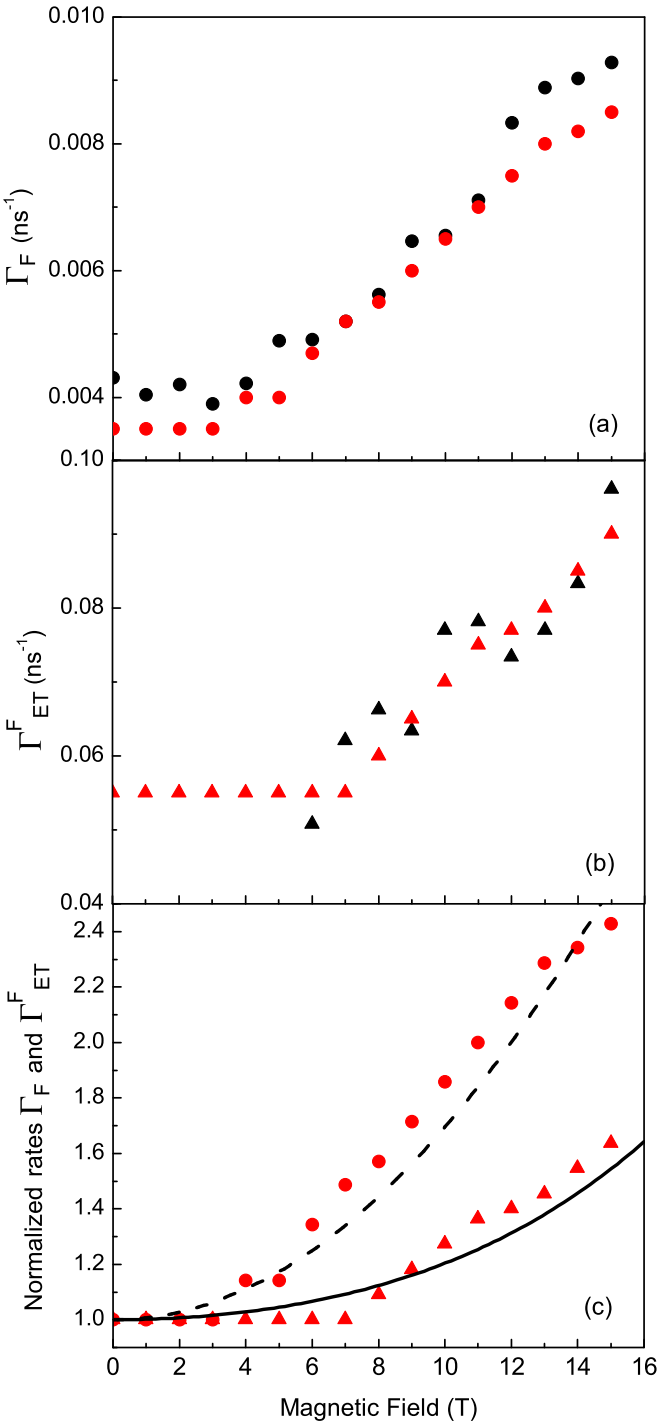

FIG. 16. (Color online) Magnetic field dependence of (a) the radiative recombination rate Γ_F and (b) the energy transfer rate of the dark exciton state Γ_{ET}^F, determined from fitting the experimental decay curves at the energy $E = E_a = 1.93$ eV using a multiexponentional form (the black symbols) and using the solution of the rate equations (the red symbols). (c) Magnetic field dependence of the normalized rates $\Gamma_{ET}^F(B)/\Gamma_{ET}^F(0)$ and $\Gamma_F(B)/\Gamma_F(0)$, determined by using the solution of the rate equations. The dashed and solid lines give fits with the magnetic field strength dependencies $\Gamma_F(B)/\Gamma_F(0) = 1 + (B/12)^2$ and $\Gamma_{ET}^F(B)/\Gamma_{ET}^F(0) = 1 + (B/12)^2 + (B/24)^4$, respectively.

Fig. 4(b)]. However, the shift of the PL maximum in the cw spectrum, $E_0 - E_m$, does not change in the external magnetic field. This fact is related to the nearly constant value of the energy transfer efficiency K_{ET} in the magnetic field and to the weak nonlinear dependence of $E_0 - E_m$ on K_{ET} in the range of large K_{ET} values [see Fig. 13(b)]. The effect of the magnetic field on the cw spectrum might become more significant in the range with smaller K_{ET} values.

It is worth to remind that the energy transfer rate $\Gamma_{ET} \propto (R_0/R_{da})^6$ [see Eq. (1)] decreases as the sixth power of the distance between the donor and acceptor NCs. Here R_0 is the characteristic Förster radius, corresponding to the FRET efficiency $K_{ET} = (R_0/R_{da})^6/[1 + (R_0/R_{da})^6] = 0.5$. That is why the energy transfer efficiency is large in the areas with high density of NCs and decreases strongly with decreasing NC density. Therefore, the areas with higher integral PL intensity correspond to areas with larger K_{ET} values and vice versa. The calculated dependence of the PL maximum shift $E_m - E_0$ on K_{ET} in Fig. 13(b) thus explains the correlation between the value of the PL maximum shift and the integral PL intensity. For example, from the PL maximum shift observed in two areas (see Fig. 2) we can estimate the change of K_{ET} from 0.9 in the high density area to 0.5 in the low density area. This corresponds to the ratio of the R_{da} values in the two areas of about 1.5. In the case when the NCs form only one layer on the substrate, this would correspond to the PL intensity ratio between the high and low density areas of about 2.25. This agrees well with the 2.5 times ratio shown in Fig. 2(a). Exploring further the modeling assumption $R_{da} \approx d$ in the high density area, we can estimate the Förster radius in the ensemble of the CdTe NCs as $R_0 \approx 5$–6 nm.

The developed theoretical model allows us to separate easily the energy region from which the initial excitation is effectively transferred and the energy region to which this excitation is transferred, by analyzing the properties of the function $T_d(E)$ constructed from the initial distribution function $N^0(E)$ and the donor probability function $f_d(E)$ according to Eq. (25). For the parameters used in Fig. 13, $T_d(E) < 0$ for $E < 2.02$ eV. Therefore, the effect of the additional PL rise caused by the energy transfer might be observed already for energies below 2.02 eV. Indeed, application of the external magnetic field allows us to observe this effect not only at lower energy part of the spectrum, but also at the centrum of the cw spectrum at 1.99 eV as can be seen in Fig. 7(e).

In conclusion, CdTe colloidal NCs have been studied by time-resolved photoluminescence in external magnetic fields. We prove that the spectral diffusion observed in emission spectra is induced by the Förster energy transfer. The energy transfer rate Γ_{ET} of an ensemble of randomly oriented CdTe NCs can be enhanced by a magnetic field. The fast relaxation of excitons from the bright to dark state as well as the admixing of the bright to the dark exciton states caused by the magnetic field results in a dominant role of the dark excitons in the FRET at low temperatures.

ACKNOWLEDGMENTS

The authors are thankful to R. A. Suris, Al. L. Efros and A. N. Poddubny for helpful discussions and to D. N. Vakhtin for the help with developing the C^{++} code. The work was partly supported by the Deutsche Forschungsgemeinschaft and the Russian Foundation of Basic Research in the frame of the ICRC TRR 160, by the Mercator Research Center Ruhr, by the Russian Foundation for Basic Research (Grant No. 13-02-00888), by the Government of Russia (project number 14.Z50.31.0021, leading scientist M. Bayer), and by the Research Grant Council of Hong Kong S.A.R. (project T23-713/11).

APPENDIX: FITTING FUNCTION FOR THE PL DECAY

If the optical excitation with a $\delta(t)$-shaped short pulse creates at $t = 0$ the populations N_i $(i = 1, \ldots, n)$ in the n exciton states, the resulting PL decay with time is given by the multiexponential function $I_\delta(t) = \sum_i I_i(t) = \sum_i \frac{C_i}{\tau_i} \exp(-\frac{t}{\tau_i})$, where τ_i is the characteristic decay time, and the amplitudes C_i are proportional to the quantum efficiency of the ith exciton state.

The shape of the laser pulse exciting the NCs in our experiment was fitted by a Gaussian function

$$I_{pulse}(t) = \frac{1}{\sigma_0\sqrt{2\pi}} \exp\left[-\frac{(t - t_0)^2}{2\sigma_0^2} \right], \tag{A1}$$

with $\sigma_0 = 0.34$ ns.

We assume at least $n = 6$ exciton states contributing to the observed PL (among them one is the upper excited state pumped by the laser pulse and one is the long-living trap state giving the background tail). The fitting function for the PL decay was obtained as the result of the following convolution:

$$\begin{aligned} I_{PL}(t) &= \int_{-\infty}^{t} I_{pulse}(T) I_\delta(t) dT \\ &= \sum_{i=0}^{5} \frac{C_i}{\tau_i} \int_{-\infty}^{t} I_{pulse}(T) \exp[-(t - T)/\tau_i] dT \\ &= \sum_{i=0}^{5} \frac{A_i}{2\tau_i} \exp\left(-\frac{t}{\tau_i} \right) \left[1 + \mathrm{Erf}\left(\frac{t - t_0}{\sqrt{2}\sigma_0} - \frac{\sigma_0}{\sqrt{2}\tau_i} \right) \right], \end{aligned} \tag{A2}$$

where $\mathrm{Erf}(x)$ is the error function and $A_i = C_i \exp(1 + \sigma_0^2/2\tau_i^2)$.

In the fitting, the negative amplitude A_1 corresponding to the initial fast rise of the PL intensity, and $1/\tau_1 = 13\ \mathrm{ns}^{-1}$ were fixed to the same values for all decay curves. The small $1/\tau_6 < 0.005\ \mathrm{ns}^{-1}$ was fixed for each decay curve individually to fit the tale of the curve in the range $I_{PL}(t)/I_{PL}(0) < 0.001$. The time $t = 0$ was set for each curve to correspond to the PL maximum, $t_0 < 0$ ($|t_0| < 1$ ns) and $I_{PL}(t_0) = 0$. The four rates $1/\tau_i > 0$ and the amplitudes A_i $(i = 2,3,4,5)$ varied within the fitting procedure which was performed with a specially developed C^{++} code. Positive amplitudes $A_i > 0$ always correspond to the decaying components, while negative amplitude $A_i < 0$ allowed us to describe the rising component in magnetic field at the low energy side of the spectrum.

[1] Edited by V. I. Klimov, *Semiconductor and Metal Nanocrystals* (Marcel Dekker, New York, 2004).

[2] Edited by A. L. Rogach, *Semiconductor Nanocrystal Quantum Dots* (Springer, Wien, 2008).

[3] D. V. Talapin, J. S. Lee, M. V. Kovalenko, and E. V. Shevchenko, Prospects of colloidal nanocrystals for electronic and optoelectronic applications, Chem. Rev. **110**, 389 (2010).

[4] A. L. Rogach, N. Gaponik, J. M. Lupton, C. Bertoni, D. E. Gallardo, S. Dunn, N. L. Pira, M. Paderi, P. Repetto, S. G. Romanov, C. O'Dwyer, C. M. S. Torres, and A. Eychmüller, Light-emitting diodes with semiconductor nanocrystals, Angew. Chem. Int. Ed. **47**, 6538 (2008).

[5] I. L. Medintz, H. T. Uyeda, E. R. Goldman, and H. Mattoussi, Quantum dot bioconjugates for imaging, labeling and sensing, Nat. Mater. **4**, 435 (2005).

[6] P. V. Kamat, Quantum dot solar cells. Semiconductor nanocrystals as light harvesters, J. Phys. Chem. C **112**, 18737 (2008).

[7] S. Rühle, M. Shalom, and A. Zaban, Quantum-dot-sensitized solar cells, Chem. Phys. Chem. **11**, 2290 (2010).

[8] C. d. M. Donega, Synthesis and properties of colloidal heteronanocrystals, Chem. Soc. Rev. **40**, 1512 (2011).

[9] N. Cicek, S. Nizamoglu, T. Ozel, E. Mutlugun, D. U. Karatay, V. Lesnyak, T. Otto, N. Gaponik, A. Eychmuller, and H. V. Demir, Structural tuning of color chromaticity through nonradiative energy transfer by interspacing CdTe nanocrystal monolayers, Appl. Phys. Lett. **94**, 061105 (2009).

[10] T. Franzl, D. S. Koktysh, T. A. Klar, A. L. Rogach, J. Feldmann, and N. Gaponik, Fast energy transfer in layer-by-layer assembled CdTe nanocrystal bilayers, Appl. Phys. Lett. **84**, 2904 (2004).

[11] C.-H. Wang, C.-W. Chen, C.-M. Wei, Y.-F. Chen, C.-W. Lai, M.-L. Ho, and P.-T. Chou, Resonant energy transfer between CdSe/ZnS type I and CdSe/ZnTe type II quantum dots, J. Phys. Chem. C **113**, 15548 (2009).

[12] A. L. Rogach, Fluorescence energy transfer in hybrid structures of semiconductor nanocrystals, Nano Today **6**, 355 (2011).

[13] S. Chanyawadee, R. T. Harley, D. Taylor, M. Henini, A. S. Susha, A. L. Rogach, and P. G. Lagoudakis, Efficient light harvesting in hybrid CdTe nanocrystal/bulk GaAs *p-i-n* photovoltaic devices, Appl. Phys. Lett. **94**, 233502 (2009).

[14] S. Chanyawadee, R. T. Harley, M. Henini, D. V. Talapin, and P. G. Lagoudakis, Photocurrent Enhancement in Hybrid Nanocrystal Quantum-Dot *p-i-n* Photovoltaic Devices, Phys. Rev. Lett. **102**, 077402 (2009).

[15] I. L. Medintz, A. R. Clapp, H. Mattoussi, E. R. Goldman, B. Fisher, and J. M. Mauro, Self-assembled nanoscale biosensors based on quantum dot FRET donors, Nat. Mater. **2**, 630 (2003).

[16] W. K. Bae, S. Brovelli, and V. I. Klimov, Spectroscopic insights into the performance of quantum dot light-emitting diodes, MRS Bull. **38**, 721 (2013).

[17] A. L. Efros, M. Rosen, M. Kuno, M. Nirmal, D. J. Norris, and M. Bawendi, Band-edge exciton in quantum dots of semiconductors with a degenerate valence band: Dark and bright exciton states, Phys. Rev. B **54**, 4843 (1996).

[18] C. R. Kagan, C. B. Murray, and M. G. Bawendi, Long-range resonance transfer of electronic excitations in close-packed CdSe quantum-dot solids, Phys. Rev. B **54**, 8633 (1996).

[19] C. R. Kagan, C. B. Murray, M. Nirmal, and M. G. Bawendi, Electronic Energy Ttransfer in CdSe Quantum Dot Solids, Phys. Rev. Lett. **76**, 1517 (1996).

[20] S. A. Crooker, J. A. Hollingsworth, S. Tretiak, and V. I. Klimov, Spectrally Resolved Dynamics of Energy Transfer in Quantum-Dot Assemblies: Towards Engineered Energy Flows in Artificial Materials, Phys. Rev. Lett. **89**, 186802 (2002).

[21] M. Achermann, M. Petruska, S. A. Crooker, and V. I. Klimov, Picosecond energy transfer in quantum dot Langmuir-Blodgett nanoassemblies, J. Phys. Chem. B **107**, 13782 (2003).

[22] J. Miyazaki and S. Kinoshita, Site-selective spectroscopic study on the dynamics of exciton hopping in an array of inhomogeneously broadened quantum dots, Phys. Rev. B **86**, 035303 (2012).

[23] F. Xu, X. Ma, C. Haughn, and J. Benavides, Efficient exciton funneling in cascaded PbS quantum dot superstructures, J. ACS Nano **5**, 9950 (2011).

[24] L. V. Poulikakos, F. Prins, and W. A. Tisdale, Transition from thermodynamic to kinetic-limited excitonic energy migration in colloidal quantum dot solids, J. Phys. Chem. C **118**, 7894 (2014).

[25] G. M. Akselrod, F. Prince, L. V. Poulikakos, E. M. Y. Lee, M. C. Weidman, A. J. Mork, A. P. Willard, V. Bulovic, and W. A. Tisdale, Subdiffusive exciton transport in quantum dot solids, Nano Lett. **14**, 3556 (2014).

[26] A. J. Mork, M. C. Weidman, F. Prins, and W. A. Tisdale, Magnitude of the Förster radius in colloidal quantum dot solids, J. Phys. Chem. C **118**, 13920 (2014).

[27] D. G. Kim, S. Okahara, M. Nakayama, and Y. G. Shim, Experimental verification of Förster energy transfer between semiconductor quantum dots, Phys. Rev. B **78**, 153301 (2008).

[28] S. F. Wuister, R. Koole, C. de Mello Donega, and A. Meijerink, Temperature-dependent energy transfer in cadmium telluride quantum dot solids, J. Phys. Chem. B **109**, 5504 (2005).

[29] R. Osovsky, A. Shavel, N. Gaponik, L. Amirav, A. Eychmúller, H. Weller, and E. Lifshitz, Electrostatic and covalent interactions in CdTe nanocrystalline assemblies, J. Phys. Chem. B **109**, 20244 (2005).

[30] M. Lunz, A. L. Bradley, W.-Y. Chen, V. A. Gerard, S. J. Byrne, Y. K. Gun'ko, V. Lesnyak, and N. Gaponik, Influence of quantum dot concentration on Förster resonant energy transfer in monodispersed nanocrystal quantum dot monolayers, Phys. Rev. B **81**, 205316 (2010).

[31] V. Rinnerbauer, H. J. Egelhaaf, K. Hingerl, P. Zimmer, S. Werner, T. Warming, A. Hoffmann, M. Kovalenko, W. Heiss, G. Hesser, and F. Schaffler, Energy transfer in close-packed PbS nanocrystal films, Phys. Rev. B **77**, 085322 (2008).

[32] O. B. Gusev, A. A. Prokofiev, O. A. Maslova, E. I. Terukov, and I. N. Yassievich, Energy transfer between silicon nanocrystals, JETP Lett. **93**, 147 (2011).

[33] A. L. Rogach, T. A. Klar, J. M. Lupton, A. Meijerink, and J. Feldmann, Energy transfer with semiconductor nanocrystals, J. Mater. Chem **19**, 1208 (2009).

[34] D. L. Dexter, A theory of sensitized luminescence in solids, J. Chem. Phys. **21**, 836 (1953).

[35] Th. Förster, Zwischenmolekulare energiewanderung und fluoreszenz, Ann. Phys. **437**, 55 (1948).

[36] J. R. Lakowicz, *Principles of Fluorescence Spectroscopy* (Kluwer Academic, New York, 1999).

[37] G. Allan and C. Delerue, Energy transfer between semiconductor nanocrystals: Validity of Försters theory, Phys. Rev. B **75**, 195311 (2007).

[38] A. N. Poddubny and A. V. Rodina (unpublished).

[39] M. Furis, J. A. Hollingsworth, V. I. Klimov, and S. A. Crooker, Time- and polarization-resolved optical spectroscopy of colloidal CdSe nanocrystal quantum dots in high magnetic fields, J. Phys. Chem. B **109**, 15332 (2005).

[40] D. E. Blumling, T. Tokumoto, K. L. Knappenberger, and S. McGill, Temperature- and field-dependent energy transfer in CdSe nanocrystal aggregates studied by magneto-photoluminescence spectroscopy, Phys. Chem. Chem. Phys. **14**, 11053 (2012).

[41] K. Becker, J. M. Lupton, J. Müller, A. L. Rogach, D. V. Talapin, H. Weller, and J. Feldmann, Electrical control of Förster energy transfer, Nat. Mater. **5**, 777 (2006).

[42] R. Vincent and R. Carminati, Magneto-optical control of Förster energy transfer, Phys. Rev. B **83**, 165426 (2011).

[43] S. Y. Kruchinin, A. V. Fedorov, A. V. Baranov, T. S. Perova, and K. Berwick, Resonant energy transfer in quantum dots: Frequency-domain luminescent spectroscopy, Phys. Rev. B **78**, 125311 (2008).

[44] A. Rodina and Al. L. Efros, Magnetic properties of nonmagnetic nanostructures: Dangling bond magnetic polaron in CdSe nanocrystals, Nano Lett. **15**, 4214 (2015).

[45] A. L. Rogach, T. Franzl, T. A. Klar, J. Feldmann, N. Gaponik, V. Lesnyak, A. Shavel, A. Eychmu, Y. P. Rakovich, and J. F. Donegan, Aqueous synthesis of thiol-capped CdTe nanocrystals: State-of-the-art, J. Phys. Chem. C **111**, 14628 (2007).

[46] F. Liu, A. V. Rodina, D. R. Yakovlev, A. Greilich, A. A. Golovatenko, A. S. Susha, A. L. Rogach, Yu. G. Kusrayev, and M. Bayer, Exciton spin dynamics of colloidal CdTe nanocrystals in magnetic fields, Phys. Rev. B **89**, 115306 (2014).

[47] J. H. Blokland, V. I. Claessen, F. J. P. Wijnen, E. Groeneveld, C. de Mello Donega, D. Vanmaekelbergh, A. Meijerink, J. C. Maan, and P. C. M. Christianen, Exciton lifetimes of CdTe nanocrystal quantum dots in high magnetic fields, Phys. Rev. B **83**, 035304 (2011).

[48] O. Labeau, P. Tamarat, and B. Lounis, Temperature Dependence of the Luminescence Lifetime of Single CdSe/ZnS Quantum Dots, Phys. Rev. Lett. **90**, 257404 (2003).

[49] L. Biadala, Y. Louyer, Ph. Tamarat, and B. Lounis, Direct Observation of the Two Lowest Exciton Zero-Phonon Lines in Single CdSe/ZnS Nanocrystals, Phys. Rev. Lett. **103**, 037404 (2009).

[50] F. Liu, L. Biadala, A. V. Rodina, D. R. Yakovlev, D. Dunker, C. Javaux, J.-P. Hermier, Al. L. Efros, B. Dubertret, and M. Bayer, Spin dynamics of negatively charged excitons in CdSe/CdS colloidal nanocrystals, Phys. Rev. B **88**, 035302 (2013).

[51] D. Thomas, J. Hopfield, and W. Augustyniak, Kinetics of radiative recombination at randomly distributed donors and acceptors, Phys. Rev. **140**, A202 (1965).

[52] V. Klimov, A. Mikhailovsky, D. McBranch, C. Leatherdale, and M. Bawendi, Quantization of multiparticle Auger rates in semiconductor quantum dots, Science **287**, 1011 (2000).